CHAPTER 2

Ternary Complex Characterization: Crystal Structures, Photophysics and Theory

2.1 Introduction

Our goal is to generate a receptor site for the detection of bacterial spores using a dipicolinate-specific lanthanide binary complex. We have chosen DO2A (*1,4,7,10*-tetraazacyclododecane-*1,7*-bisacetate) as the chelating ligand because this macrocycle binds lanthanides with high affinity and leaves three adjacent coordination sites available on the Ln^{3+} ion for the tridentate DPA to bind. Prior to qualifying our lanthanide complexes as dipicolinate receptor sites, we must fully characterize the corresponding $Ln(DO2A)(DPA)^-$ ternary complexes for the various luminescent lanthanides (samarium, europium, terbium and dysprosium). This will involve structural and spectroscopic analyses to determine how parameters such as ligand bond length, luminescence quantum yield and hydration number vary across the series, in addition to theoretical studies to better understand any trends we may find. We expect that structural variations will follow with lanthanide ionic radius, but that the terbium and europium complexes will exhibit the greatest luminescence intensities due close coupling between the DPA triplet energy level and the lanthanide excited state.

2.2 Structural Characterization

2.2.1 Crystallization

Crystallization of the ternary $Ln(DO2A)(DPA)^-$ complexes (Ln = Sm, Eu, Gd, Tb and Dy) is necessary to produce pure compound for accurate quantum yield calculation and analysis of binding properties, as well as to confirm complex formation through crystallographic analysis. The energy gaps between the emissive excited states and the ground state manifolds for Sm^{3+} and Dy^{3+} are 7,400 cm^{-1} and 7,850 cm^{-1}, respectively, significantly less than those of Tb^{3+} and Eu^{3+}.[1] However, these lanthanides are still capable of sensitized emission in the visible range, and due to their difference in ionic radii (nearly 5 pm difference from Sm^{3+} to Dy^{3+}) are of interest in structural characterization and binding studies.[2] Similarly, though gadolinium complexes cannot be used in luminescence experiments, crystals of $Gd(DO2A)(DPA)^-$ will provide additional structural information in terms of any trends due to lanthanide ionic radius. Reported here are the first structurally characterized ternary lanthanide(macrocycle)(dipicolinate) complexes.

Experimental Section

Materials. The following chemicals were purchased and used as received: acetone (J. T. Baker), acetonitrile (Fluka Biochemika), ammonium hydroxide (28.0–30.0% in water) (J. T. Baker), DPA (dipicolinic acid, pyridine-*2,6,*-dicarboxylic acid) (Aldrich), dysprosium(III) chloride hydrate (Alfa Aesar), ether anhydrous (Acros Organics), ethyl alcohol (200-proof) (Acros Organics), europium(III) chloride hexahydrate (Aldrich), hydrochloric acid (36.5–38.0% in water) (EMD Chemicals), methanol (J. T. Baker), samarium(III) chloride (Alfa Aesar), sodium hydroxide (NaOH 50% in water) (Mallinckrodt), terbium(III) chloride hexahydrate (Alfa Aesar), terbium(III) nitrate hexahydrate (Aldrich), tetrabutylammonium chloride hydrate (Aldrich), tetrabutylammonium hydroxide (TBAOH 10% in *2*-propanol) (TCI America), tetrabutylammonium hydroxide (TBAOH 40% in water) (TCI America), and tetraphenyl-arsonium(V) chloride hydrate (Aldrich). All lanthanide salts were 99.9% pure or greater, all solvents were ACS certified or HPLC grade, and all other salts were 97% pure or greater. Water was deionized to a resistivity of 18.2 MΩ-cm using a Purelab® Ultra laboratory water purification system (Siemens Water Technologies, Warrendale, PA).

The *1,4,7,10*-tetraazacyclododecane-*1,7*-diacetate (DO2A) ligand was prepared by hydrolysis of *1,4,7,10*-tetraazacyclododecane-*1,7*-di(*tert*-butyl acetate) (DO2A-tBu-ester) (Macrocyclics, Dallas, TX).[3] The DO2A-tBu-ester (4.8334 g, 12.07 mmol), a slightly off-white powder, was dissolved in 120 mL of 20% hydrochloric acid in a roundbottom flask and refluxed for 24 hours with stirring in an oil bath (115 °C). The hydrochloric acid was removed by rotary evaporation under vacuum (~ 50 mbar) in a hot water bath (55 °C) for approximately 5 hours to give a white solid. The deprotected ligand was then rinsed using a fine frit (Pyrex, 15 mL, ASTM 4-5.5F, No. 36060) and vacuum filtration with the following in sequence: 50 mL of absolute ethanol (200-proof), 10 mL of diethyl ether, 20 mL of an ethanol-ether (1:1) mixture, and three 20-mL aliquots of ether. The solid was dried in a dessicator under vacuum for five days to produce $DO2A\cdot 2.80HCl\cdot 0.85H_2O$ (4.6745 g, 11.53 mmol) in 94.84% yield. Anal. Calcd (found) for $C_{12}H_{24}N_4O_4\cdot 2.80HCl\cdot 0.85H_2O$ (fw = 405.57): C, 35.54 (35.54); H, 7.08 (6.72); N, 13.81 (13.25); Cl, 24.43 (25.10).

Methods. Initial crystallization attempts of the $Tb(DO2A)(DPA)^-$ ternary complex involved addition of equimolar amounts of terbium chloride hexahydrate, dipicolinic acid and DO2A to a small volume (5.0 mL) of nanopure water (18.2 MΩ-cm resistivity). The pH was adjusted to ~ 8 with 50% sodium hydroxide added dropwise. The solution was vortexed and sonicated for approximately 1 minute until fully dissolved, filtered using a sterile Acrodisc® 25 mm syringe filter with a 0.2 μm Supor® membrane (Pall Corporation, Ann Arbor, MI), separated into 1-mL aliquots and set aside for crystal formation. Though crystals were observed, the high solubility of the Tb(DO2A)(DPA) sodium salt in aqueous solution led to crystal formation only as the solution evaporated to dryness. The resulting crystals therefore had a white surface residue, presumably excess reactants and sodium chloride, which caused elemental and mass spectrometry analyses to be inconsistent with the solved crystal structure. Attempts to remove the residue with washing steps completely dissolved the crystals. Substitution of terbium nitrate for terbium chloride, or sodium dipicolinate (Na_2DPA) for dipicolinic acid, produced similar results. New solvent systems had to be explored.

Subsequent crystallization attempts included experimentation with various solvents (methanol, ethanol, acetonitrile), counterions (sodium hydroxide, ammonium hydroxide, tetraphenylarsonium chloride, tetrabutylammonium chloride), filters (0.2 μm syringe filters, glass wool, Pyrex fine and medium frits) and reaction conditions (pH, temperature). Components were combined in aqueous solution, and following confirmation of ternary complex formation by fluorescence spectroscopy, the solutions were lyophilized using a MicroModulyo Freeze Dryer (Thermo Electron Corporation, Waltham, MA) to dryness. The solid was then resuspended in the desired solvent and filtered prior to slow evaporation at a specified temperature. In all cases, only precipitates were observed. As with the aqueous case, the high solubility of the ternary complex salts in methanol resulted in precipitation only upon going to dryness, so this solvent was abandoned as well.

It was hypothesized that the use of both a strong base and a counterion salt to adjust solution pH and provide a cation for $Tb(DO2A)(DPA)^-$, respectively, was forming other salts with greater propensities to crystallize or form a precipitate. Therefore, the pH adjustment base and counterion salt were combined into one reagent to minimize the extraneous ions in solution. Instead of using sodium hydroxide in conjunction with tetrabutylammonium chloride to produce the tetrabutylammonium (TBA) salt of Tb(DO2A)(DPA), for example, only tetrabutylammonium hydroxide (TBAOH) was added, eliminating the potential to form sodium salts that might interfere with crystallization of the ternary complex. It should also be noted that *only* the TBAOH in isopropanol resulted in crystal formation; performing the identical procedure with TBAOH in water resulted in precipitation. This may indicate that isopropanol is a critical component in the unit cell (see Section 2.2.2). Fluorescence and gravimetric studies revealed that the TBA·Tb(DO2A)(DPA) salt had greater solubility in acetone than in acetonitrile, ethanol, or mixtures of acetonitrile and ethanol (5%, 10% and 20% ethanol). Acetone therefore became the solvent of choice, and ultimately produced crystals of sufficient size and quality for high resolution diffraction studies. It should finally be noted that only *new* frits produced crystals of high quality; a previously-used frit, even if only used once under identical conditions for the same crystallization, would result in poor quality crystals or a precipitate. Attempts to clean the frits using exhaustive rinsing in several solvents, various acid digests or kilning did not resolve the issue. It is therefore recommended that the procedure be performed with care and adjusted to produce sufficient sample, as a new frit must be used each time.

Equimolar aliquots of $TbCl_3 \cdot 6H_2O$ (0.18974 g, 0.508 mmol) and $DO2A \cdot 2.80HCl \cdot 1.00H_2O$ (0.20738 g, 0.508 mmol) were dissolved in 3.00 mL of nanopure water (18.2 MΩ-cm resistivity) using gentle heating (40 °C) and sonication. The white cloudy mixture became clear and colorless upon clarification. The pH of the solution was adjusted to ~ 6 with tetrabutylammonium hydroxide (TBAOH, 10% in 2-propanol) added dropwise, and the solution was allowed to equilibrate with stirring and gentle heating for at least 2 hours to promote complete formation of the $Tb(DO2A)^+$ complex. A slightly smaller aliquot of DPA (0.08176 g, 0.489 mmol) was then added to the solution, along with 11.00 mL of nanopure H_2O. This is to prevent formation of any $Tb(DPA)_n$ species ($1 \leq n \leq 3$). The pH of the solution was adjusted to 8.5 with TBAOH, added dropwise. Addition of the yellow TBAOH solution caused formation of a white precipitate, but clarification was observed with stirring and gentle heating in under 5 minutes. The clear, yellow solution was lyophilized using a MicroModulyo Freeze Dryer for 6 days, and 20.0 mL of acetone was added to the resulting orange solid, which was sonicated and vortexed to solubilize as much of the ternary complex as possible. The mixture was centrifuged at 8000 rpm (25 ºC) for 20 minutes (Model 5810 R, Eppendorf, Hamburg, Germany), and the yellow/orange supernatant was quickly and carefully decanted from the white pellet. The supernatant was filtered through a new fine frit (Pyrex, 15 mL, ASTM 4-5.5F) under vacuum with a bell jar directly into a clean scintillation vial (rinsed 3 times with filtered acetone to remove any particulates that might cause multiple nucleation sites). Crystal formation was observed after sitting at room temperature for 24 hours. Suitable crystals were utilized for X-ray diffraction studies at the Beckman Institute X-ray Crystallography Facility (Caltech), while the rest were dried over P_2O_5 under vacuum for 7 days and delivered to: (1) Desert Analytics Transwest Geochem for elemental analysis, and (2) the mass spectrometer facility at Caltech.

Elemental analysis. Elemental analysis was performed in duplicate with determination of carbon, hydrogen, nitrogen and the lanthanide of interest. The CHN protocol is based on analysis using the Dumas method,[4] where combustion and oxidation with a WO_3 catalyst converts carbon, hydrogen and nitrogen to CO_2, H_2O and NO_X, respectively. The NO_X is reduced to N_2 and the gases are separated using a packed column prior to detection via thermal conductivity. Metal prep involves acid digestion and detection via inductively coupled argon plasma atomic emission spectroscopy (ICAP-AES).

Mass spectrometry. Dried crystals were dissolved in methanol and the mass spectrum obtained using a LCQ Finnigan MAT electrospray ionization mass spectrometer (ESI-MS) in negative ion mode.

Results and Discussion

The same procedure developed for $Tb(DO2A)(DPA)^-$ was used to produce crystals of the samarium, europium, gadolinium and dysprosium ternary complexes as tetrabutylammonium salts. Detailed characterization of each batch of crystals is provided (vide infra). Low yields are due to the relatively low solubility of the complex in acetone, as evidenced by a significant percentage of precipitate remaining after centrifugation. As the focus of this crystallization was on quality as opposed to quantity, the yield was not optimized.

TBA·Sm(DO2A)(DPA). 0.474 g, yield: 44.8%. Anal. Calcd (found) in duplicate for $NC_{16}H_{36}\cdot SmC_{19}H_{25}N_5O_8\cdot 3.29H_2O\cdot 0.21C_{16}H_{36}NCl$ (fw = 960.8): C, 47.88 (47.80); H, 7.87 (7.40); N, 9.05 (9.32); Sm, 15.65 (15.65). ESI-MS (*m/z*): calcd (found) for $SmC_{19}H_{25}N_5O_8$ (M^-) 603.4 (603.1).

TBA·Eu(DO2A)(DPA). 0.269 g, yield: 38.9%. Anal. Calcd (found) in duplicate for $NC_{16}H_{36}\cdot EuC_{19}H_{25}N_5O_8\cdot 3.52H_2O\cdot 0.93C_{16}H_{36}NCl$ (fw = 1168.8): C, 51.32 (51.33); H, 8.77 (8.00); N, 8.31 (8.49); Eu, 13.00 (12.95). ESI-MS (*m/z*): calcd (found) for $EuC_{19}H_{25}N_5O_8$ (M^-) 604.4 (604.1).

TBA·Gd(DO2A)(DPA). 0.158 g, yield: 19.8%. Anal. Calcd (found) in duplicate for $NC_{16}H_{36}\cdot GdC_{19}H_{25}N_5O_8\cdot 3.3H_2O\cdot 1.8C_3H_6O\cdot 0.3HCl$ (fw = 1027.7): C, 47.36 (47.37); H, 7.74 (7.41); N, 8.18 (8.70); Gd, 15.30 (15.30); Cl, 0.95 (0.95). TOF-MS ES (*m/z*): calcd (found) for $Gd_1C_{19}H_{25}N_5O_8$ (M^-) 609.0944 (609.0947).

TBA·Tb(DO2A)(DPA). 0.301 g, yield: 42.3%. Anal. Calcd (found) in duplicate for $NC_{16}H_{36}\cdot TbC_{19}H_{25}N_5O_8\cdot 1.00C_3H_6O\cdot 4.00H_2O$ (fw = 982.97): C, 46.43 (46.63); H, 7.69 (8.17); N, 8.55 (8.71); Tb, 16.17 (15.65). ESI-MS (*m/z*): calcd (found) for $TbC_{19}H_{25}N_5O_8$ (M^-) 610.4 (610.1).

TBA·Dy(DO2A)(DPA). 0.102 g, yield: 45.4%. Anal. Calcd (found) in duplicate for $NC_{16}H_{36}\cdot DyC_{19}H_{25}N_5O_8\cdot 9.24H_2O\cdot 1.45C_{16}H_{36}NCl$ (fw = 1426.9): C, 49.04 (49.05); H, 9.31 (7.66); N, 7.32 (8.68); Dy, 11.39 (11.40). ESI-MS (*m/z*): calcd (found) for $Dy_1C_{19}H_{25}N_5O_8$ (M^-) 615.4 (615.1).

Even in acetone, the crystals were visibly luminescent under UV excitation with a handheld UVGL-25 multiband UV lamp (UVP, Upland, CA) in short wave (254 nm) and long wave (365 nm) modes. The terbium crystals displayed green luminescence, the europium crystals had red emission, dysprosium a faint yellow and samarium a dim pink (Figure 2.1). Once dry, the crystals became opaque and much more luminescent under UV irradiation, presumably due to loss of solvent from the unit cell.

2.2.2 X-ray Crystallography

All five TBA·Ln(DO2A)(DPA) complexes will be analyzed to determine ligand chelation motif and the corresponding bond lengths and angles. The DO2A ligand should coordinate in a hexadentate fashion, with the tridentate dipicolinate ligand occupying the remaining three coordination sites on the Ln^{3+} ion. We anticipate slight variations due to the lanthanide contraction as we go from the largest Sm^{3+} ion to the smallest Dy^{3+} ion in the series of five lanthanides investigated.

Experimental Section

Methods. Diffraction data for the Sm, Eu, Tb and Dy crystals were collected at 100 ± 2 K on a Bruker SMART 1000 CCD area detector diffractometer equipped with graphite monochromated MoKα radiation ($\lambda\alpha = 0.71073$ Å). A Bruker KAPPA APEX II diffractometer was utilized for the Gd crystals at the same temperature and wavelength. To reduce solvent loss, all crystals were coated in a layer of epoxy prior to mounting and data collection.

The structures were solved by direct methods for the Sm, Eu, and Gd complexes and isomorphous methods for the Dy complex using SHELXS-97.[5] The Tb structure was solved by direct methods using Bruker XS (version 6.12).[6] All complexes were refined by full-matrix least-squares calculations on F^2 against all reflections using the Direct Bruker XL (Tb)[7] or SHELXL-97 (Sm, Eu, Gd, Dy) program packages.[8, 9] Non-hydrogen atoms were refined anisotropically. The hydrogen atoms were introduced in calculated positions. CCDC reference numbers 655647 (Sm), 634507 (Eu), 746157 (Gd), 629354 (Tb) and 643596 (Dy). Crystal and refinement data are collected in Table 2.1. Complete crystallographic data for all five complexes, including asymmetric unit contents, atomic coordinates, bond distances and angles, and anisotropic displacement parameters, is listed in Appendix D.

Results and Discussion

With the exception of europium, all Ln(DO2A)(DPA)$^-$ complexes crystallized in the monoclinic space group P2_1/c, indicating a primitive lattice with an inversion center. The unit cell has a 2_1 screw axis, meaning a two-fold rotation (180°) followed by a translation of ½ of the lattice vector in the direction of symmetry. This space group also has a glide plane along the c-axis, signifying a translation along half the lattice vector orthogonal to the direction of symmetry.[10] The Eu(DO2A)(DPA)$^-$ complex crystallized in the triclinic space group P1, indicating a primitive lattice with no symmetry. Though this is a different space group in Hermann-Mauguin notation,[11, 12] all five ternary complexes are crystallographically isostructural, with slight differences (< 0.05 Å) appearing to follow the trend of Ln^{3+} ionic radius (Figures 2.2, 2.3). The difference in space groups is attributed to the fact that the solvent region of the unit cell in all structures was disordered, containing acetone/isopropanol, ethanol and water.

As anticipated, in all five structures the lanthanide is complexed in a 9-coordinate fashion between the tridentate DPA and hexadentate DO2A ligands, and solvent is completely excluded from the Ln^{3+} coordination sphere. The coordination geometry of the lanthanide in each structure can be described as a slightly distorted capped staggered square bipyramidal conformation, with a pseudo-C2 axis passing through the DO2A core, the lanthanide and the DPA nitrogen (Figure 2.4). Although there are four possible stereoisomers of the lanthanide-cyclen compound,[13, 14] only Δ(λλλλ) or Λ(δδδδ) is observed in the asymmetric unit. On average, the Ln--N interatomic distances for the DO2A ligand are slightly shorter than reported values for similar macrocyclic lanthanide complexes, whereas the Ln--O distances are slightly longer (Table 2.2).[15] This may indicate that the lanthanide ion is sitting more deeply in the DO2A macrocycle ring, which is supported by a slight decrease in the N-Ln-O bite angle for the coordinated carboxylate 'arms' from 66.4° in Eu(DOTA) to 65.9° in the Eu(DO2A)(DPA)$^-$ complex.[15] In contrast to the DOTA case, the Ln--N distances for the DO2A ligand are also no longer equivalent; the two substituted aza nitrogens are ~ 0.08 Å closer than the two nitrogens lacking coordinating arms. Similar distortions (0.04 – 0.05 Å) have been reported for DO3A derivatives coordinated to Tb^{3+} and Eu^{3+}.[16]

The crystal structure for calcium dipicolinate trihydrate contains the DPA ligand in a planar configuration.[17] However, all five crystal structures of the Ln(DO2A)(DPA)$^-$ complex show a slight torsion of the carboxylate oxygens coordinated to the lanthanide out of the plane of symmetry. Though this might indicate a steric interaction between the dipicolinate and macrocyclic ligands, this distortion does not appear to hinder dipicolinate coordination; Ln--O and Ln--N distances for DPA are within the range reported for the terbium tris(dipicolinate) complex (± 0.01 Å).[18]

2.2.3 Temperature Dependence

Crystals of TBA·Tb(DO2A)(DPA) and TBA·Eu(DO2A)(DPA) will be studied at temperatures of 100, 200 and 300 K to determine if any discernable temperature dependence exists in bond lengths and/or angles of the crystal structures.

Experimental Section

Methods. Crystals were mounted on a glass fiber using Paratone oil, coated in epoxy and placed on the diffractometer under a nitrogen stream at the designated temperature. Diffraction data were collected at 100 ± 2 K, 200 ± 2 K and 300 ± 2 K on a Bruker KAPPA APEX II diffractometer equipped with graphite monochromated MoKα radiation ($\lambda\alpha = 0.71073$ Å). For each complex, the same crystal was used for all three temperatures. The structures were solved by direct methods using SHELXS-97 and refined by full-matrix least-squares calculations on F^2 against all reflections using the SHELXL-97 program package. Non-hydrogen atoms were refined anisotropically.

For the Eu complex, the asymmetric unit contained acetone at one site that was disordered between two orientations; this site was refined as a rigid body starting with the coordinates from the 100 K structure. Hydrogen atoms on water were located in the electron density difference map and were constrained to ride the appropriate oxygen. All other hydrogens were placed at geometric positions and refined as riding atoms. No other restrains were placed on the model. CCDC reference numbers 761599 (100 K), 762705 (200 K) and 763335 (300 K). Crystal and refinement data are collected in Table 2.3. Complete crystallographic data for all three complexes, including asymmetric unit contents, atomic coordinates, bond distances and angles, and anisotropic displacement parameters, is listed in Appendix E.

Results and Discussion

As temperature increases from 100 K to 300 K, the Ln--DPA distance decreases slightly (0.01 Å) and the Ln--DO2A distance increases by approximately the same margin for both the Tb and Eu complexes. This trend with temperature only appears to affect the Ln^{3+} coordination to the macrocyclic ring; the Ln--O distances of the carboxyl arms do not change. We attribute most of the observed shift to libration, and conclude that if there is a temperature dependence in the crystal structures of the TBA· Ln(DO2A)(DPA) complexes, it is negligible.

2.3 Photophysics

2.3.1 Spectroscopy

While absorption spectroscopy can provide some information about complexes involving dipicolinate, this technique does not tell us much about the lanthanides due to the forbidden nature of f–f transitions. Fluorescence spectrophotometry, in contrast, can reveal the symmetry of the lanthanide coordination sphere, the extent of sensitization by the chromophore and whether solvent deactivation is a significant source of quenching.

Experimental Section

Materials. The following chemicals were purchased and used as received: DPA (dipicolinic acid, pyridine-*2,6,*-dicarboxylic acid) (Aldrich), deuterium oxide 99.9% (Cambridge Isotope Laboratories, Inc.), dysprosium(III) chloride hydrate (Alfa Aesar), europium(III) chloride hexahydrate (Aldrich), nitric acid (EMD Chemicals, Inc.), samarium(III) chloride (Alfa Aesar), sodium acetate trihydrate (Mallinckrodt), sodium hydroxide (NaOH 50% in water) (Mallinckrodt), terbium(III) chloride hexahydrate (Alfa Aesar), tris buffer (tris-[hydroxymethyl]aminomethane) (MP Biomedicals, LLC) and L-tryptophan (Alfa Aesar). DO2A was prepared as previously described (Section 2.2.1).

Methods. Stock solutions of LnDPA and $Ln(DPA)_3$ were prepared gravimetrically by addition of the lanthanide chloride salt to 0.9 or 10 equivalents of dipicolinate, respectively, and dilution in nanopure water (18.2 MΩ-cm resistivity). Stock solutions of ternary complex were prepared gravimetrically from dried TBA·Ln(DO2A)(DPA) crystals of known molecular weight (Section 2.2.1). These stock solutions were diluted to 10.0 μM in 0.1 M Tris buffer (pH 7.9, adjusted with 50% NaOH added dropwise) or 0.2 M sodium acetate (pH 7.4, adjusted with 50% NaOH added dropwise). All solutions were allowed to equilibrate for at least 24 hours prior to analysis.

Absorbance measurements were made in quartz cuvettes (1 cm path length) using a Cary 50 Bio UV/Visible Spectrophotometer (Varian, Inc., Palo Alto, CA), and luminescence measurements, also in quartz, were performed using a Fluorolog-3 Fluorescence Spectrometer (Horiba Jobin-Yvon, Edison, NJ). To prevent the second-order diffraction of the source radiation, a 350-nm cutoff filter (03 FCG 055, Melles Griot, Covina, CA) was used in all luminescence measurements. All reported spectra were obtained as a ratio of corrected signal to corrected reference (S_c/R_c), where the reference is a separate photodiode detector, to eliminate the effect of varying background radiation in the sample chamber (Figure 2.5). Reported intensities are in units of counts per second per microampere (cps/μA).

Results and Discussion

Absorbance, luminescence excitation (λ_{Sm} = 600 nm, λ_{Eu} = 615 nm, λ_{Tb} = 544 nm, λ_{Dy} = 574 nm) and emission (λ_{ex} = 278 nm) spectra were obtained for each ternary complex (excluding Gd). The UV absorption spectra of all four complexes (Figure 2.6) revealed peaks at 271 and 278 nm, attributable to the $\pi \rightarrow \pi^*$ transitions of bound DPA.[19] Luminescence excitation and emission spectra (Figures 2.7–2.10) are consistent with a DPA → Ln^{3+} energy transfer mechanism, where the most intense emission occurs at 601 nm ($^4G_{5/2} \rightarrow {}^6H_{7/2}$) for the Sm complex, 617 nm ($^5D_0 \rightarrow {}^7F_2$) for the Eu complex, 545 nm ($^5D_4 \rightarrow {}^7F_5$) for the Tb complex and 484 nm ($^4F_{9/2} \rightarrow {}^6H_{15/2}$) for the Dy complex.[20-23]

To confirm that the observed increase in luminescence upon dipicolinate coordination is due to an absorption-energy transfer-emission (AETE) mechanism and not simply exclusion of solvent molecules from the lanthanide coordination sphere, the emission spectra of the Tb aquo ion was recorded in H_2O and in D_2O. Deuterated water has a greater mass and therefore a lower O–D oscillator frequency, meaning it does not participate in nonradiative deactivation through vibronic quenching as normal O–H oscillators in water do. The $Tb^{3+}\cdot 9D_2O$ species therefore represents the unquenched lanthanide luminescence in solution, whereas $Tb^{3+}\cdot 9H_2O$, with O–H oscillators comprising the entire coordination sphere, represents the most severely quenched species. Though there is a marked increase (threefold) in luminescence of the Tb^{3+} cation when in deuterated solvent, this is almost negligible in comparison to the effect of one dipicolinate ligand (Figure 2.11). If the only function of tridentate DPA binding were to displace three water molecules from the Tb^{3+} coordination sphere, the intensity should be a factor of three lower than the $Tb^{3+}\cdot 9D_2O$ spectrum, which has displaced all nine waters. The nearly 3-orders-of-magnitude increase in luminescence is clear evidence of lanthanide sensitization via the AETE mechanism.

It is quite curious that the dipicolinate anion alone exhibits no detectable fluorescence.[24] Though the sodium and calcium salts of DPA emit very weak fluorescence in the 400–420 nm range when excited around 300 nm,[25] the DPA^{2-} anion has no detectable fluorescent signal, despite theoretical studies which suggest otherwise.[19] We have verified this same result in a variety of solvents (H_2O, acetonitrile, dichloromethane, toluene). Though the reasons why the dipicolinate anion is invisible are still unknown, this adds an advantage of reduced fluorescent background in terms of developing a luminescence-based assay for DPA.

The ternary complex emission spectra all display unique band splittings that are dependent on the site symmetry of the lanthanide coordination sphere, including those of Sm^{3+} ([Xe] $4f^5$) and Dy^{3+} ([Xe] $4f^9$), which exhibit Kramers' degeneracy in low symmetry cases such as this (see Section 2.4.1).[26] For all four lanthanides this splitting is present in all observable emission peaks, regardless of hypersensitivity (i.e., the $^5D_0 \rightarrow {}^7F_2$ transition of Eu^{3+}), degeneracy of the lanthanide ground state, or whether assigned as electric dipole or magnetic dipole transitions. For example, emission spectra of the mono $Tb(DPA)^{+}\cdot 6H_2O$ complex, the homoleptic $Tb(DPA)_3^{3-}$ species, and ternary $Tb(DO2A)(DPA)^{-}$ all exhibit very different splittings, and these characteristic differences can be used to visually identify the major component in solution.

2.3.2 Quantum Yields

Using absorbance and fluorescence measurements in tandem, it is possible to quantitatively measure the efficiency of lanthanide sensitization in our complexes. For our purposes, 'quantum yield' refers to the luminescence quantum yield (Φ_L), defined as the ratio of photons absorbed (by the chromophore) to photons emitted through luminescence (by the lanthanide). Therefore, Φ_L represents the probability of formation of the lanthanide the excited state via the absorption-energy transfer-emission (AETE) mechanism, coupled to the probability of the excited state being deactivated by luminescence as opposed to non-radiative deactivation pathways. Several deactivation pathways can cause this value to be significantly less than unity, such as inefficient coupling of the chromophore triplet energy level to the lanthanide excited state, or vibrational quenching from solvent molecules in or near the lanthanide coordination sphere. Typically, a compound with a quantum yield greater than 0.1 is considered to be quite luminescent.

Experimental Section

Methods. Five concentrations ranging from 5.0 to 15.0 μM were prepared for each lanthanide complex (excluding Gd) in 0.1 M Tris buffer (pH 7.9). Absorbance and luminescence measurements were made in quartz cuvettes (1 cm path length) using a Cary 50 Bio UV/Visible Spectrophotometer, and a Fluorolog-3 Fluorescence Spectrometer (λ_{ex} = 280 nm). Absorbance measurements were zeroed to an empty quartz cuvette in the sample chamber; quartz cuvettes containing solvent only were run in triplicate as a control, so no baseline correction was necessary. All recorded absorbances were under 0.1 and all luminescence intensities were below 5 x 10^5 cps (counts per second), well within the linear range of both instruments. Quartz cuvettes were cleaned using a nitric acid (50% in nanopure water) digest and rinsed thoroughly with nanopure water between samples. No background fluorescence was observed for the solvents used.

The quantum yield of each complex was calculated using the following equation:

$$\Phi_X = \Phi_{ST} \cdot \frac{\mathrm{Grad}_X}{\mathrm{Grad}_{St}} \cdot \frac{I_{ST}(\lambda_{ST})}{I_X(\lambda_X)} \cdot \frac{\eta_X^2}{\eta_{ST}^2} \qquad [2.1]$$

where Φ is quantum yield, X is the sample, ST is the standard, I is the intensity of the excitation light at wavelength λ and η is the refractive index of the solvent. 'Grad' refers to the gradient relationship in equation 2.2 obtained by plotting data as integrated luminescence emission intensity (E) against absorbance (A).

$$\mathrm{Grad} = \frac{E}{A} \qquad [2.2]$$

Emission spectra were plotted as intensity against energy (cm^{-1}) and integrated using the FluorEssence software package. Quantum yield measurements were standardized to L-tryptophan in deionized water (18.2 MΩ-cm resistivity) at the same excitation wavelength, pH 5 (Φ_{ref} = 0.13 ± 0.01).[27] Corrections were made for the difference in refractive index between buffered H_2O (0.1 M Tris) and pure H_2O. Molar extinction coefficients were also calculated for the ternary complexes and the dipicolinate anion by plotting absorbance against concentration (Figure 2.12).

We attempted to use $Cs_3[Eu(DPA)_3]$ as our secondary standard, which was reported by Chauvin et al.[28, 29] to have a quantum yield of 24 ± 2.5% (λ_{ex} = 279 nm) at 75 μM in 0.1 M Tris buffer. $Cs_3[Eu(DPA)_3]$ was prepared as described by Brayshaw et al.[30] 9.73 g, yield: 96.2%. Anal. Calcd (found) in duplicate for $Cs_3Eu_1C_{21}N_3O_{12}H_9\cdot 26.4H_2O\cdot Cs_2CO_3$ (fw = 1215.7): C, 22.29 (22.29); H, 5.13 (2.08); N, 3.46 (3.71); Eu, 12.50 (12.50). However, this concentration of $Cs_3[Eu(DPA)_3]$ has an absorbance around 1.0 with a 1 cm path length cell, not in the 0.2 range as was described. In order to obtain absorbances in the proper linear range, the concentration of the $Cs_3[Eu(DPA)_3]$ had to be decreased to 5.0 μM. This was problematic, as the stability constant of $Eu(DPA)_3^{3-}$ is in this range (3.1 μM).[31] We believe that the authors must have used 0.2 cm path length cells, and that these should be used for any quantum yield experiments involving tris-DPA lanthanide complexes as secondary standards. Otherwise, the $Eu(DPA)_3^{3-}$ complex dissociates to $Eu(DPA)_2^{-}$ and DPA^{2-}, and emission intensity no longer tracks linearly with absorbance (Figure 2.13). As we were using 1 cm path length cells, we simply discarded this standard in favor of the more accepted L-tryptophan.

Results and Discussion

Molar extinction coefficients for the four luminescent ternary complexes and the dipicolinate anion are all in the same range of 10^3 $M^{-1}cm^{-1}$, which is expected as all contain the same amount of chromophore, the only strongly absorbing species (Table 2.4). The calculated molar extinction coefficient of the tryptophan standard ($\varepsilon_{Exp} = 5277$ $M^{-1}cm^{-1}$) was within 5% of the reported value ($\varepsilon_{Exp} = 5502$ $M^{-1}cm^{-1}$).[27]

The luminescence quantum yields for Tb complexes are greater than those of the Dy, Eu, and Sm complexes (Table 2.5). This is most likely due to (1) the small energy gap and corresponding strong coupling between the DPA triplet state and the terbium $^5D_4$ excited state[22, 32, 33] and (2) the absence of other terbium excited states lower in energy than the DPA triplet, which might quench emission via nonradiative decay.[34] Samarium and europium have larger energy gaps between accepting energy levels and the DPA triplet level,[35, 36] so intensity loss in these lanthanide complexes is probably due to poor coupling and lack of efficient energy transfer (Table 2.6). For the case of Dy, the quantum yield is lower despite an even smaller energy gap,[37] because the $^4I_{15/2}$ and $^4G_{11/2}$

excited states are also populated and each contributing to the loss of quantum yield via nonradiative decay.[35] The high efficiency and intensity of the Tb complex suggests that $Tb(DO2A)^+$ is the optimal choice as a dipicolinate receptor site.

2.3.3 Lifetime Measurements

Luminescence lifetimes of lanthanide complexes can provide information about the coordination environment and degree of quenching of the lanthanide in solution. According to the Judd-Ofelt theory of lanthanide photophysics, the radiative lifetimes of Laporte-forbidden f–f transitions should be on the order of milliseconds.[38-40] However, reported experimental decay lifetimes for lanthanide complexes are significantly faster (microseconds), suggesting that non-radiative transitions have considerable influence on radiative lifetimes in these complexes.[41]

As described in Chapter 1, non-radiative relaxation due to solvent interactions can severely reduce lanthanide luminescence due to energy dissipation by vibronic modes, with the O–H oscillator being the most common and efficient quencher. However, if these O–H oscillators are replaced with low-frequency O–D oscillators, the efficiency of the vibronic deactivation pathway decreases substantially. Therefore, the rate constants for luminescence lifetimes (τ_{H_2O}) of lanthanide excited states in water or alcoholic solvents are often much shorter than those in the analogous deuterated solvents (τ_{D_2O}). This property can be utilized to determine the degree of solvation for luminescent lanthanides with a fair amount of certainty.

The hydration number, or the number of bound water molecules in the lanthanide coordination sphere, can be calculated using a method derived by Horrocks and Sudnick for terbium and europium complexes.[42] The relationship between Tb or Eu excited-state lifetimes (τ) experimentally determined in H_2O and D_2O solvents, and the hydration number (q) is given in equation 2.3.

$$q = A_{Ln}\left(\frac{1}{\tau_{H_2O}} - \frac{1}{\tau_{D_2O}}\right) \qquad [2.3]$$

All lifetimes are in milliseconds, and the A_{Ln} constant is a proportionality factor specific to a given lanthanide which takes into account the energy gap between the ground and excited state manifolds. For example, A_{Tb} is 4.2 ± 0.5 ms while A_{Eu} is only 1.05 ± 0.5 ms. This equation was later modified by Parker et al. to produce equation 2.4, which takes into account quenching effects from coordinated N–H oscillators (where ‘x’ is the number of N–H oscillators) and outer sphere water molecules.[43]

$$\begin{aligned} q^{Eu} &= A_{Eu}\left[\left(\frac{1}{\tau_{H_2O}} - \frac{1}{\tau_{D_2O}}\right) - 0.25 - 0.075x\right] \\ q^{Tb} &= A_{Tb}\left[\left(\frac{1}{\tau_{H_2O}} - \frac{1}{\tau_{D_2O}}\right) - 0.06 - 0.0056x\right] \end{aligned} \qquad [2.4]$$

The effect of the DO2A ligand, which contains two N–H oscillators, results in a proportionality factor of 4.6 ± 0.5 ms when coordinated to Tb^{3+}, assuming slow exchange with D_2O.[44]

Experimental Section

Materials. Deuterium oxide 99.9% (Cambridge Isotope Laboratories, Inc.), DPA (dipicolinic acid, pyridine-*2,6,*-dicarboxylic acid) (Aldrich), sodium hydroxide (NaOH 50% in water) (Mallinckrodt), and terbium(III) chloride hexahydrate (Alfa Aesar) were purchased and used as received. DO2A was prepared as previously described (Section 2.2.1).

Methods. All samples were prepared in triplicate to a final volume of 4.00 mL with 1 mM NaOH (pH 7.5) in nanopure water (18.2 MΩ-cm resistivity) in disposable acrylate cuvettes (Spectrocell, Oreland, PA), 1 cm path length, and were allowed to equilibrate for at least 24 hours prior to analysis. Complex formation was verified using the characteristic profiles of the various emission spectra obtained on a Fluorolog-3 Fluorescence Spectrometer. Samples to be investigated in D_2O were prepared in the same manner and then dried in a dessicator with Drierite (W. A. Hammond Drierite Co., Ltd., Xenia, OH) under vacuum for at least 7 days. The solid precipitate in these cuvettes was redissolved in D_2O by gentle mixing immediately prior to analysis. The solution pH/pD was checked using a calibrated handheld pH/mV/temperature meter (Model IQ150, I. Q. Scientific Instruments, Loveland, CO) following data collection.

A modified Fluorolog 3-τ spectrofluorometer (Horiba Jobin-Yvon, Edison, NJ) was used for lifetime measurements at 25 °C (Figure 2.14.). The fourth harmonic generation (λ_{ex} = 266 nm) of a 10 nanosecond pulsed Quanta Ray Lab Series neodymium-doped yttrium aluminum garnet (Nd:YAG) laser (Newport Corp, Irvine, CA) was used as the excitation source, with output of the photomultiplier tube (PMT) detector digitized using an oscilloscope to obtain plots of voltage against time (Figure 2.15). The laser power was adjusted to 1.0 mW to avoid heating the sample or destroying the acrylate cuvettes. Lifetime decay curves were fit to a monoexponential curve of the form in equation 2.5 using the Kaleidagraph software package.

$$I(t) = C + I_0 e^{-t/\tau} \qquad [2.5]$$

In this fit, I is the signal intensity (measured in volts), I_0 is the initial or maximum signal intensity, t is the time in seconds, τ is the lifetime in seconds and C is a constant to adjust for background intensity due to scatter in the sample chamber. The hydration number (q) for each terbium complex was then calculated using equation 2.3, with $A_{Tb} = 4.6$ or 4.2 ± 0.5 ms per bound water molecule for complexes with and without DO2A, respectively.

Results and Discussion

Luminescence lifetime measurements of the various terbium complexes indicate a significant increase in lifetime in D_2O compared to H_2O, as expected due to quenching from vibronic coupling (Table 2.7). The lifetime of the terbium dipicolinate complex in water (0.6 ms) is consistent with the values reported by Jones and Vullev at a similar pH (0.599 ms).[45] Further, the hydration number of each complex is within range of what was expected assuming Tb^{3+} is 9-coordinate, and indeed, a value of q = 8.8 was calculated for the terbium-aquo complex. The $Tb(DO2A)^+$ complex, containing the hexadentate DO2A ligand, had a hydration number of 2.4, which is consistent with reported values of q = 3.0 and 2.6 inner-sphere water molecules for $Eu(DO2A)(H_2O)_q^+$ and $Eu(DO2A)(OH)(H_2O)_{q-1}$, respectively.[46] The very low hydration number (q = 0.3) for the $Tb(DO2A)(DPA)^-$ ternary complex indicates exclusion of water from the terbium coordination sphere, and is consistent with the high quantum yield of this complex, which no longer experiences quenching effects due to inner-sphere vibronic deactivation.

2.4 Theoretical Investigations

2.4.1 Crystal Field Theory: Europium as an Example

As described in Chapter 1, lanthanide emission profiles have complex character due to Stark sublevel splitting, which is largely dependent on the site symmetry of the central lanthanide ion. Thus, if the emission spectrum of a pure lanthanide complex (or the absorption spectrum for lanthanide-doped single crystals) is known, it is in principle possible to determine the point group of the lanthanide site, even in solution.[47] However, the group theory and resulting crystal-field parameterization of lanthanides is significantly more complex than transition metals, and complications such as low site symmetry or the additional degeneracy of odd-electron lanthanides make spectral assignment of crystal-field transitions even more difficult. Systems with an odd number of f-electrons (i.e., Sm^{3+}, Gd^{3+} and Dy^{3+}) are nearly impossible to use as probes for the site symmetry around the lanthanide ion due to Kramer's degeneracy.[26] For a complex with symmetry lower than cubic, every ${}^{2S+1}L_J$ level will be split into J + ½ crystal-field levels in the absence of an external magnetic field. A progressive lowering of the site symmetry will thus not result in a progressive removal of the 2J + 1 fold degeneracy of the ${}^{2S+1}L_J$ level. We therefore focus on lanthanides with an even number of f-electrons for our analysis of site symmetry in lanthanide complexes.

The europium ion has several characteristics that make it ideal for use as a probe of site symmetry. First, Eu^{3+} has an even number of electrons ([Xe] $4f^6$), so total degeneracy is removed in low symmetry cases. Second, the $^7F_0$ ground state of Eu^{3+} is non-degenerate, meaning it will transform as the totally symmetric representation of the point group, which simplifies spectral interpretation significantly. Third, many of the $^{2S+1}L_J$ levels where J is small (and there is a straightforward relationship between crystal-field splitting and crystal-field parameters) are present in the optical region for europium, meaning crystal field parameters can be measured directly from experimental spectra. Finally, there is very little overlap between the crystal-field levels of different J states, so levels in the ground ^7F_J and excited ^5D_J terms can be easily distinguished in high-resolution spectra. We can therefore use our europium complexes to validate lanthanide site symmetries in solution against what is observed in the crystal structure.

For this exercise, we focus on the $Eu(DPA)_3^{3-}$ and $Eu(DO2A)(DPA)^-$ complexes, for which the point groups are known from the crystal structures. The $Eu(DO2A)(DPA)^-$ complex crystallized in a geometry best described by the C_2 point group (see Section 2.2.2) . Though no crystal structure of the $Eu(DPA)_3^{3-}$ complex has been reported, the analogous $Tb(DPA)_3^{3-}$ complex has been crystallized as the sodium salt; the three tridentate dipicolinate ligands arranged in a D_3 fashion around the terbium ion.[18] This symmetry is supported by absorption measurements of the $Eu(DPA)_3^{3-}$ complex in solution.[48] Using high-resolution emission spectra of these two complexes, we can qualitatively determine the point group of each in solution and compare to that found in the corresponding crystal structures.

The most interesting and informative transitions in the europium luminescence spectrum are: $^5D_0 \rightarrow {}^7F_0$ (580 nm), $^5D_0 \rightarrow {}^7F_1$ (595 nm), $^5D_0 \rightarrow {}^7F_2$ (615 nm) and $^5D_0 \rightarrow {}^7F_4$ (695 nm). All of these are electric dipole transitions with the exception of $^5D_0 \rightarrow {}^7F_1$, which is a magnetic dipole transition.[26] The first peak in the emission spectrum allows for determination of sample purity and significantly narrows down the list of potential point groups. If the $^5D_0 \rightarrow {}^7F_0$ transition shows any splitting whatsoever, more than one non-equivalent site is present. This transition is also reported to shift with coordination number, most likely due to an increase in Eu^{3+}-ligand covalency via the nephelauxetic effect.[49, 50] Further, according to the selection rules for electric dipole transitions, this transition can only be present in cases of C_{nv}, C_n or C_s symmetry. Therefore, if this peak is absent, the symmetry around the Eu^{3+} ion is high.

The next peak, usually found around 595 nm, allows for further isolation of the correct point group of the complex. If the $^5D_0 \rightarrow {}^7F_1$ transition is split into three peaks, the symmetry must be either orthorhombic (D_2, C_{2v}), monoclinic (C_2, C_s) or triclinic (C_1). If the transition has only two peaks, we are left with hexagonal, trigonal or tetragonal symmetries.

If the symmetry is high, more transitions are forbidden by symmetry restrictions; therefore, lanthanides occupying sites of low symmetry will have more peaks within a spin-orbit coupling band than those in site of higher symmetry. This feature is well illustrated by the $^5D_0 \rightarrow {}^7F_2$ (615 nm) transition. If the symmetry is found to be orthorhombic, monoclinic or triclinic, the point group can be mostly ferreted out using this transition. If the band at 615 nm has only three peaks, the point group is D_2, four peaks indicate a point group of C_{2v}, and five peaks leave the remaining point groups (C_2, C_s and C_1) as possibilities. For the hexagonal, trigonal and tetragonal symmetries, further information is required. If polarized spectra can be obtained, distinctions can be made using this and the $^5D_0 \rightarrow {}^7F_4$ transition to clearly identify the point group of the Eu^{3+} coordination sphere (Figure 2.16).

Each transition of the emission spectra for $Eu(DPA)_3^{3-}$ and $Eu(DO2A)(DPA)^-$ were deconvoluted into a sum of Gaussians to quantify the number of peaks in each band (Figure 2.17). For the europium tris(dipicolinate) complex, we find the $^5D_0 \rightarrow {}^7F_0$ transition is absent and the $^5D_0 \rightarrow {}^7F_1$ transition is split into two peaks, indicating a point group of higher symmetry (hexagonal, trigonal or tetragonal). We can also see that the intense $^5D_0 \rightarrow {}^7F_2$ transition is split into only two peaks which, despite the fact that we cannot identify polarizability in this spectrum, is strong evidence for the D_3 point group. The analysis of crystal field splitting of the $Eu(DPA)_3^{3-}$ emission spectrum therefore implies that the europium ion is in a similar configuration in both the crystal structure and in solution, and that this configuration is best described by the D_3 point group.

For the ternary complex, we clearly identify a single peak for the $^5D_0 \rightarrow {}^7F_0$ transition, meaning our sample has low symmetry and high purity. The position of this peak at 581 nm (17,215 cm^{-1}) indicates a 9-coordinate environment around the Eu^{3+} central ion.[49] The triply-split $^5D_0 \rightarrow {}^7F_1$ transition confirms orthorhombic, monoclinic or triclinic symmetry. Finally, the $^5D_0 \rightarrow {}^7F_2$ transition is split into 5 peaks, narrowing down the possibilities to C_1, C_2 or C_s. Cursory analysis of the $Eu(DO2A)(DPA)^-$ emission spectrum using selection rules of specific transitions is therefore in close agreement with the crystal structure, which purports a point group of C_1 or C_2 for this complex. Hence, the coordination sphere of the Eu^{3+} ion appears to remain consistent in terms of symmetry from solid state to solution.

Our theoretical investigation using europium as an example suggests that the symmetries observed in the crystal structures of $Eu(DPA)_3^{3-}$ and $Eu(DO2A)(DPA)^-$ are preserved when these complexes are in solution. Though systematic structural studies of various lanthanide complexes have shown that it can be rather difficult to satisfactorily extrapolate what is observed in the solid state to behavior in solution, in some cases the gross aspects such as symmetry are retained.[51-53] While not necessarily conclusive, this exercise serves to demonstrate the potential of crystal field theory to validate experimental data for lanthanide complexes that are well characterized.

2.4.2 Density Functional Theory

To better understand the energetics of the $Ln(DO2A)(DPA)^-$ ternary complex and dipicolinate binding to $Ln(DO2A)^+$, a collaboration was established with John A. Keith, Josef Anton and Timo Jacob at the University of Ulm, Germany, to perform density functional theory (DFT) calculations on this system.

Calculations were run with the PBE0 hybrid method (a variant of the PBE generalized-gradient exchange-correlation functional including exact Hartree exchange) with Tb^{3+} as the central lanthanide. The number of atoms within these complexes prevented practical simulation of the highest-accuracy basis sets. Instead, the CSDZ pseudopotential was used on the lanthanide while all other atoms used the double-zeta quality 6-31G** basis set. As these were relatively high-spin complexes, calculations used the restricted open-shell Hartree-Fock (ROHF) method; spin-polarized unrestricted Hartree-Fock (UHF) calculations found near-identical energies as minimal spin contamination was found at the minimum energy spin state. After pre-optimization in vacuum, the geometric structures were then optimized under the constraints of a self-consistent reaction field (SCRF) continuum method to model a surrounding water solvent. Energy values (E_{SCF} and E_{solv}) were recalculated with more expansive triple-zeta basis sets to minimize basis set superposition errors (BSSEs). Density functional methods are known to poorly describe long- and medium-range vdW contributions, and to address the importance of these terms, they were explicitly calculated with a semiempirical approach[54] prior to computation of ΔΔE for all reactions.

Computational results indicated only two solvent molecules in the terbium coordination sphere for the $Tb(DO2A)^+$ complex, even after full optimization in solvent (Figure 2.18). This is consistent with reported hydration states of $Ln(DO2A)(H_2O)_n$ complexes, with $n = 3$ for Ce through Eu and $n = 2$ for Tb to Yb,[55] though our lifetime measurements suggest a slightly higher hydration number for this complex.

Further computational investigations found very similar relative binding energies for all Ln complexes, not in agreement with our experimental results. For a given binding constant k_n, the binding energy is given by equation 2.6.

$$k_n = \frac{kT}{h} \cdot e^{-\Delta G_n / kT} \qquad [2.6]$$

For detection of two binding constants (k_1 and k_2) within a factor of 100, we can determine the minimum allowable difference in ΔG for a given temperature by substituting and solving as shown in equation 2.7.

$$\begin{aligned}
&\frac{k_1}{k_2} = 100 \\
&\frac{\frac{kT}{h} \cdot e^{-\Delta G_1/kT}}{\frac{kT}{h} \cdot e^{-\Delta G_2/kT}} = 100 \\
&e^{(\Delta G_2 - \Delta G_1)/kT} = 100 \\
&(\Delta\Delta G) = \ln(100) \cdot kT
\end{aligned} \qquad [2.7]$$

At 298 K, kT = 0.592 kcal/mol. Substituting in this value and solving for ΔΔG, we have equation 2.8.

$$\Delta\Delta G = 2.73 \text{ kcal/mol} \qquad [2.8]$$

We therefore must have computational accuracy within 3.0 kcal/mol to accurately detect two binding constants within a factor of 100. Since similar calculations are capable of errors from 2-5 kcal/mol for small organics, let alone for substantially more complicated lanthanide complexes, it would not be surprising if the standard computational approach could not successfully discern binding constants within this order, and a more advanced approach is necessary.

One likely possibility is the lack of rigorous treatment of relativistic effects and spin-orbit coupling; treatment of these effects was the motivation for the collaboration with the Ulm group. Unfortunately, the highly polarizable dipicolinate ligand was found to cause convergence errors in the Ulm code, and an accurate theoretical model of the ternary complex could not be obtained (energetics within 5 kcal/mol). Since these errors could not lead to an improvement over the previously used model, further understanding of these complexes from theory could not be obtained.

2.5 Conclusions

Five Ln(DO2A)(DPA)$^-$ ternary complexes, where Ln = Sm, Eu, Gd, Tb and Dy, were successfully crystallized as tetrabutylammonium salts by slow evaporation out of acetone. Crystallographic analysis revealed the structures were all isostructural and superimposable, with slight differences following the trend of lanthanide ionic radius. Variation of temperature from 100 to 300 K resulted in negligible differences in the crystal structures of the Tb and Eu complexes.

Excitation and absorption spectra of the four luminescent complexes (Sm, Eu, Tb and Dy) were very similar, with two $\pi \rightarrow \pi^*$ transitions at 271 and 278 nm. Emission spectra confirm sensitized luminescence via the AETE mechanism for all four complexes, with emission intensities in the order of Tb >> Eu >> Dy > Sm. Quantum yield measurements verify optimal energy transfer efficiency in the Tb^{3+} complex, most likely due to close coupling between the dipicolinate triplet energy level and the terbium $^5D_4$ excited state.

Lifetime measurements of various Tb^{3+} complexes indicate nine waters bound in the aquo complex, six in the Tb(DPA)$^+$ complex, and two to three in the Tb(DO2A)$^+$ complex. The fully formed Tb(DO2A)(DPA)$^-$ complex excludes solvent completely from the lanthanide coordination sphere.

Analysis of Stark splitting in the europium emission spectra using selection rules corroborates point group assignments of D_3 and C_1/C_2 for the Eu(DPA)$_3^{3-}$ and Eu(DO2A)(DPA)$^-$ complexes, respectively, suggesting symmetry is conserved when such complexes are in solution. Theoretical calculations using density functional theory (DFT) were found to be limited and inconsistent with experimental results.

With the ternary complexes fully characterized in terms of their structure and photophysics, we may begin to approach the Ln(DO2A)$^+$ series in terms of receptor site design. The complex that is most effective as a dipicolinate sensor will be validated with real bacterial spores both from laboratory and environmental samples.

REFERENCES

(1) Brunet, E.; Juanes, O.; Rodriguez-Ubis, J. C. *Current Chemical Biology* **2007**, *1*, 11-39.

(2) Cotton, S. *Lanthanide and Actinide Chemistry*; John Wiley & Sons Ltd.: West Sussex, England, 2006.

(3) Huskens, J. *Inorganic Chemistry* **1997**, *36*, 1495-1503.

(4) Sweeney, R. A.; Rexroad, P. R. *Journal of AOAC International* **1987**, *70*, 1028-1030.

(5) Sheldrick, G. M. *Acta Crystallographica* **1990**, *A46*, 467-473.

(6) 6.12 ed.; Bruker-AXS: Madison, WI, 2001.

(7) 6.12 ed.; Bruker-AXS: Madison, WI, 2001.

(8) Sheldrick, G. M.; University of Göttingen: Göttingen, Germany, 1997.

(9) Sheldrick, G. M. *Acta Crystallographica* **2008**, *A64*, 112-122.

(10) Sands, D. E. In *Introduction to Crystallography*; Dover Publications, Inc.: Mineola, New York, 1993, pp 47-165.

(11) Hermann, C., Ed. *Internationale Tabellen zur Bestimmung von Kristallstrukturen. I. Band*, 1 ed.: Borntrager, Berlin, 1935.

(12) Dewolff, P. M.; Billiet, Y.; Donnay, J. D. H.; Fischer, W.; Galiulin, R. B.; Glazer, A. M.; Hahn, T.; Senechal, M.; Shoemaker, D. P.; Wondratschek, H.; Wilson, A. J. C.; Abrahams, S. C. *Acta Crystallographica Section A* **1992**, *48*, 727-732.

(13) Thompson, M. K.; Lough, A. J.; White, A. J. P.; Williams, D. J.; Kahwa, I. A. *Inorganic Chemistry* **2003**, *42*, 4828-4841.

(14) Moreau, J.; Guillon, E.; Aplincourt, P.; Pierrard, J.-C.; Rimbault, J.; Port, M.; Aplincourt, M. *European Journal Of Inorganic Chemistry* **2003**, *2003*, 3007-3020.

(15) Chang, C. A.; Francesconi, L. C.; Malley, M. F.; Kumar, K.; Gougoutas, J. Z.; Tweedle, M. F. *Inorganic Chemistry* **1993**, *32*, 3501-3508.

(16) Gunnlaugsson, T.; Harte, A. J.; Leonard, J. P.; Nieuwenhuyzen, M. *Supramolecular Chemistry* **2003**, *15*, 505-519.

(17) Strahs, G.; Dickerson, R. E. *Acta Crystallographica Section B* **1968**, *24*, 571-578.

(18) Van Meervelt, L.; Binnemans, K.; Van Herck, K.; Görller-Walrand, C. *Bulletin des Sociétés Chimiques Belges* **1997**, *106*, 25-27.

(19) Hameka, H. F.; Jensen, J. O.; Jensen, J. L.; Merrow, C. N.; Vlahacos, C. P. *Journal of Molecular Structure (Theochem)* **1996**, *365*, 131-141.

(20) Sabbatini, N.; Guardigli, M.; Bolletta, F.; Manet, I.; Ziessel, R. *Angewandte Chemie-International Edition In English* **1994**, *33*, 1501-1503.

(21) Bünzli, J.-C. G. *Lanthanide probes in life, chemical and earth sciences: Theory and practice*; Elsevier: New York, 1989.

(22) Latva, M.; Takalo, H.; Mukkala, V.-M.; Matachescu, C.; Rodriguez-Ubis, J. C.; Kankare, J. *Journal Of Luminescence* **1997**, *75*, 149-169.

(23) Rudzinski, C. M.; Engebretson, D. S.; Hartmann, W. K.; Nocera, D. G. *Journal of Physical Chemistry A* **1998**, *102*, 7442-7446.

(24) Barela, T. D.; Sherry, A. D. *Analytical Biochemistry* **1976**, *71*, 351-352.

(25) Nudelman, R.; Bronk, B. V.; S., E. *Applied Spectroscopy* **2000**, *54*, 445-449.

(26) Görller-Walrand, C.; Binnemans, K. In *Handbook on the Physics and Chemistry of Rare Earths*; Gschneidner, J., K. A., Eyring, L., Eds.; Elsevier Science B. V.: New York, 1996; Vol. 23, pp 122-283.

(27) Chen, R. F. *Analytical Letters* **1967**, *1*, 35 - 42.

(28) Chauvin, A. S.; Gumy, F.; Imbert, D.; Bunzli, J. C. G. *Spectroscopy Letters* **2004**, *37*, 517-532.

(29) Chauvin, A. S.; Gumy, F.; Imbert, D.; Bunzli, J. C. G. *Spectroscopy Letters* **2007**, *40*, 193-193.

(30) Brayshaw, P. A.; Bunzli, J. C. G.; Froidevaux, P.; Harrowfield, J. M.; Kim, Y.; Sobolev, A. N. *Inorganic Chemistry* **1995**, *34*, 2068-2076.

(31) Grenthe, I. *Journal Of The American Chemical Society* **1961**, *83*, 360-364.

(32) Arnaud, N.; Vaquer, E.; Georges, J. *Analyst* **1998**, *123*, 261-265.

(33) Sharma, P. K.; Van Doorn, A. R.; Staring, A. G. J. *Journal of Luminescence* **1994**, *62*, 219-225.

(34) Carnall, W. T.; Fields, P. R.; Rajnak, K. *Journal Of Chemical Physics* **1968**, *49*, 4447-4449.

(35) Carnall, W. T.; Fields, P. R.; Rajnak, K. *Journal Of Chemical Physics* **1968**, *49*, 4424-4442.

(36) Carnall, W. T.; Fields, P. R.; Rajnak, K. *Journal Of Chemical Physics* **1968**, *49*, 4450-4455.

(37) Hemmila, I.; Laitala, V. *Journal Of Fluorescence* **2005**, *15*, 529-542.

(38) Judd, B. R. *Physical Review* **1962**, *127*, 750-761.

(39) Ofelt, G. S. *Journal Of Chemical Physics* **1962**, *37*, 511-520.

(40) Walsh, B. M. In *Advances in Spectroscopy for Lasers and Sensing*; Di Bartolo, B., Forte, O., Eds.; Springer: The Netherlands, 2006, pp 403-433.

(41) Sabbatini, N.; Guardigli, M.; Lehn, J. M. *Coordination Chemistry Reviews* **1993**, *123*, 201-228.

(42) Horrocks Jr., W. D.; Sudnick, D. R. *Journal Of The American Chemical Society* **1979**, *101*, 334-340.

(43) Beeby, A.; Clarkson, I. M.; Dickins, R. S.; Faulkner, S.; Parker, D.; Royle, L.; de Sousa, A. S.; Williams, J. A. G.; Woods, M. *Journal of the Chemical Society-Perkin Transactions 2* **1999**, 493-503.

(44) Parker, D.; Williams, J. A. G. *Journal Of The Chemical Society-Perkin Transactions 2* **1995**, 1305-1314.

(45) Jones, G.; Vullev, V. I. *Photochemical & Photobiological Sciences* **2002**, *1*, 925-933.

(46) Chang, C. A.; Chen, Y.-H.; Chen, H.-Y.; Shieh, F.-K. *Journal Of The Chemical Society-Dalton Transactions* **1998**, 3243-3248.

(47) Sinha, S. P.; Butter, E. *Molecular Physics* **1969**, *16*, 285-298.

(48) Binnemans, K.; Van Herck, K.; Görller-Walrand, C. *Chemical Physics Letters* **1997**, *266*, 297-302.

(49) Choppin, G. R.; Wang, Z. M. *Inorganic Chemistry* **1997**, *36*, 249-252.

(50) Frey, S. T.; Horrocks Jr., W. D. *Inorganica Chimica Acta* **1995**, *229*, 383-390.

(51) Shestakova, A. K.; Chertkov, V. A.; Schneider, H.-J.; Lysenko, K. A. *Organic Letters* **2001**, *3*, 325-327.

(52) Aime, S.; Barge, A.; Botta, M.; Fasano, M.; Ayala, J. D.; Bombieri, G. *Inorganica Chimica Acta* **1996**, *246*, 423-429.

(53) Harrowfield, J. M. In *Metal Ions in Biological Systems: The Lanthanides and Their Interrelations with Biosystems*; Sigel, A., Sigel, H., Eds.; Marcel Dekker, Inc.: New York, 2003; Vol. 40, pp 105-159.

(54) Grimme, S. *Journal of Computational Chemistry* **2006**, *27*, 1787-1799.

(55) Yerly, F.; Dunand, Frank A.; Tóth, É.; Figueirinha, A.; Kovács, Z.; Sherry, A. D.; Geraldes, C. F. G. C.; Merbach, André E. *European Journal Of Inorganic Chemistry* **2000**, *2000*, 1001-1006.

FIGURES

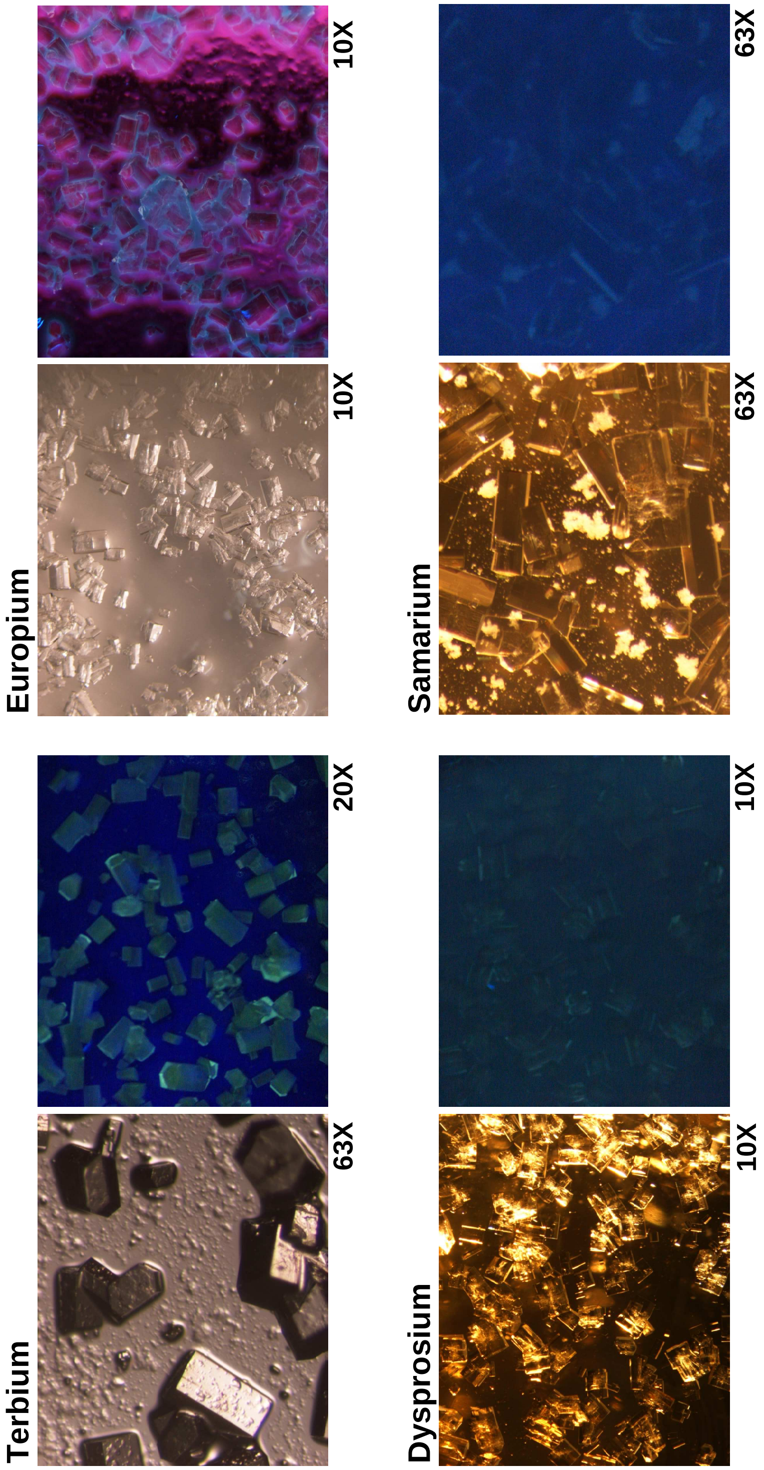

Figure 2.1. Photos of TBA·Ln(DO2A)(DPA) crystals (Ln = Tb, Eu, Dy and Sm). In each pair, image at left is under normal illumination, image at right under UV excitation at 365 nm. Images taken using a Nikon SMZ800 optical microscope. Magnifications indicated below each image.

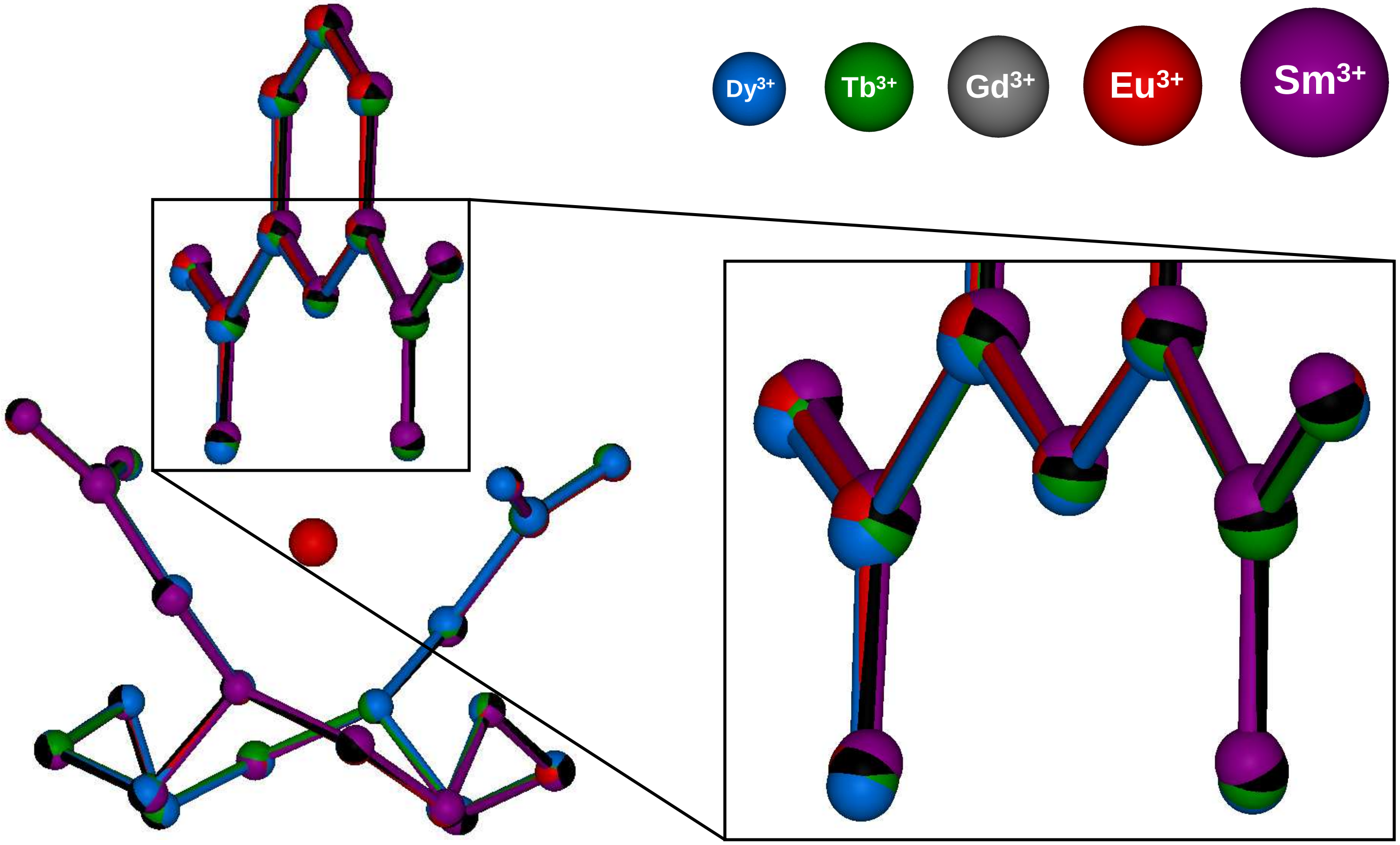

Figure 2.2. Comparison of Ln(DO2A)(DPA)$^-$ crystal structures, where Ln = Sm, Eu, Gd, Tb and Dy. All five ternary complexes are almost perfectly superimposable; in these views, structures have been tethered via the lanthanide and the four nitrogens of the DO2A ring. The slight trend of extension following lanthanide ionic radius is visible in the upward shift of the DPA ligand from Dy to Sm (inset). Legend of lanthanide ions (upper right) are exaggerated in size to illustrate the trend of ionic radius.

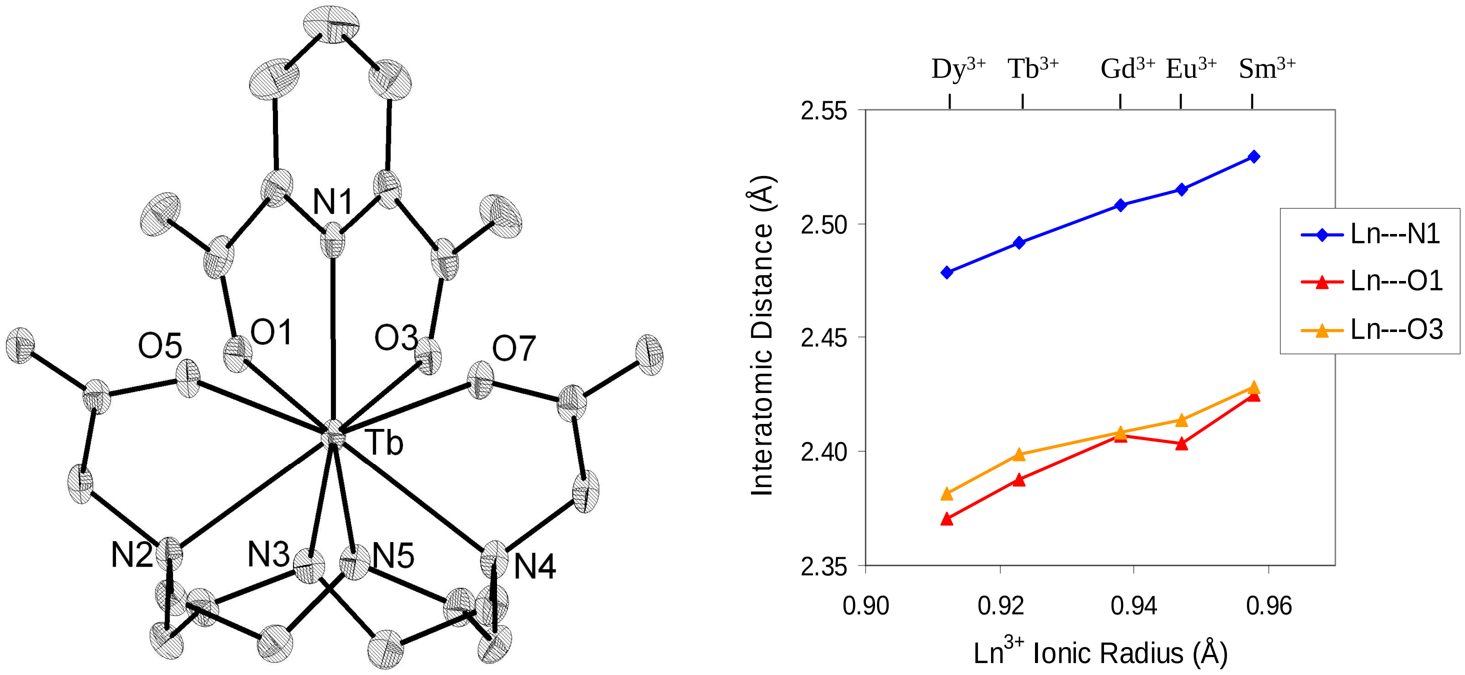

Figure 2.3. Ternary complex expansion due to lanthanide ionic radius. Left: Thermal ellipsoid plot of the Tb(DO2A)(DPA)$^-$ ternary complex with 50% probability. Hydrogens omitted for clarity. Right: Plot of Ln^{3+}--DPA interatomic distances for the five ternary complex crystal structures against Ln^{3+} ionic radius. Trivalent ionic radius values from S. Cotton, Lanthanide and Actinide Chemistry, John Wiley & Sons Ltd., 2006.

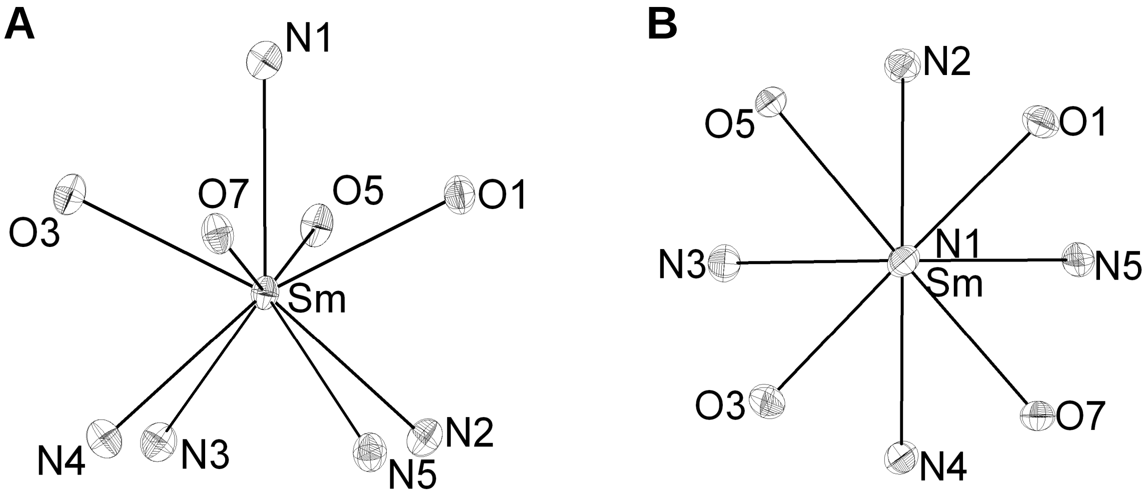

Figure 2.4. Geometry of the lanthanide coordination site in the Tb(DO2A)(DPA)$^{-}$ complex. Thermal ellipsoid plots (50% probability) of the samarium coordination sphere show the capped square bipyramidal geometry, with the four DO2A nitrogens in the lower plane and four oxygens (two from DPA, two from DO2A) in the upper plane. (A) Looking across the complex, with DO2A below and DPA above the Sm^{3+} central ion. (B) Looking down the DPA ligand (the N1 of the DPA is obstructing the view of the Sm).

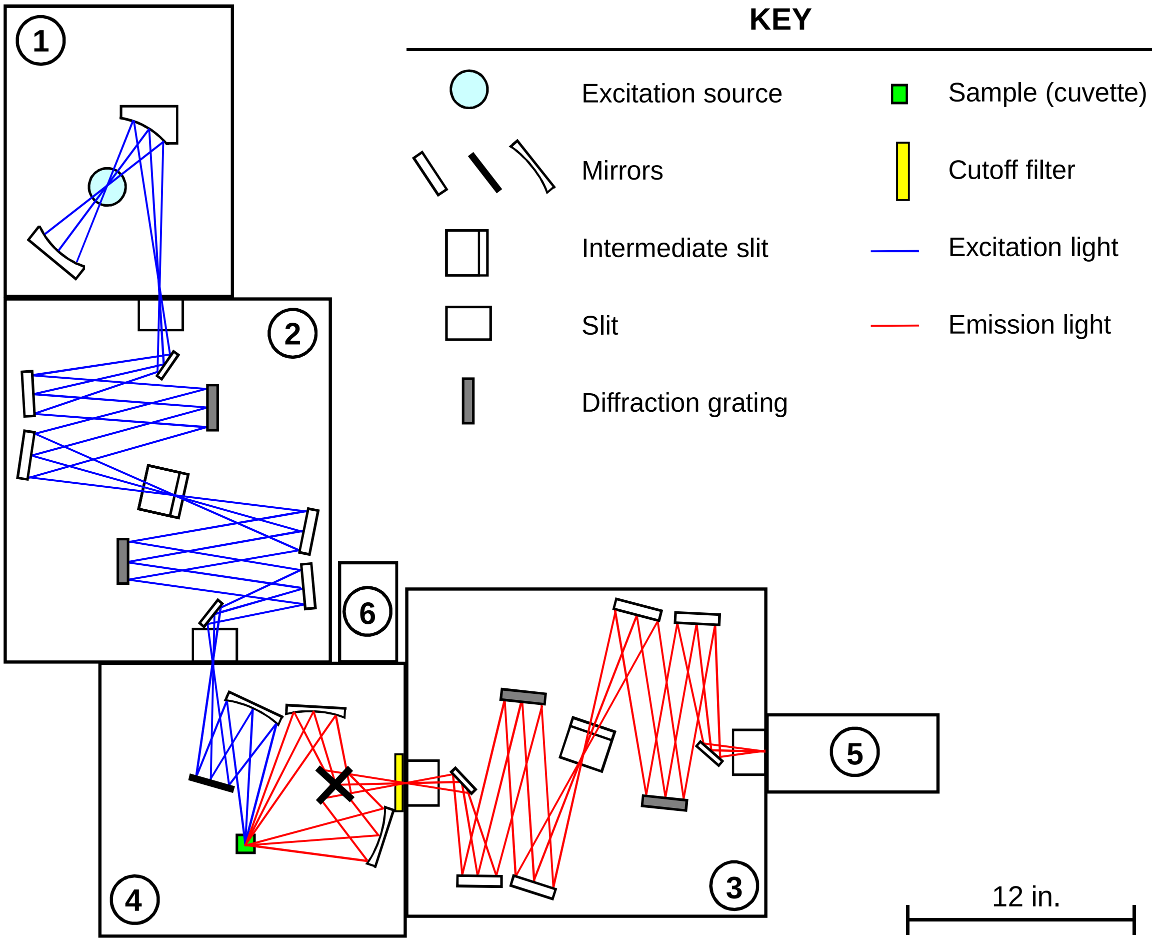

Figure 2.5. Schematic of the Fluorolog-3 Model FL3-22 spectrofluorometer. The instrument is comprised of interchangeable modules arranged in an 'L' configuration. The light source is a 450-W xenon short-arc lamp (1) mounted vertically in an air-cooled housing. Wavelength selection is accomplished using Czerny-Turner double-grating monochromators for excitation (2) and emission (3) light with all-reflective optics and 0.5-nm accuracy. The sample chamber (4) is temperature-controlled and adjustable for right-angle or front-face detection. This model has two detectors: the primary signal detector is a R928P photomultiplier tube (5) thermoelectrically cooled with a Peltier cooling unit, and the reference detector is a photodiode (6). The 350-nm cutoff filter (yellow) is positioned between the sample chamber and the emission double monochromator module. The hardware is directed by a SpectrAcq controller and the user interface is managed by the FluorEssence software package.

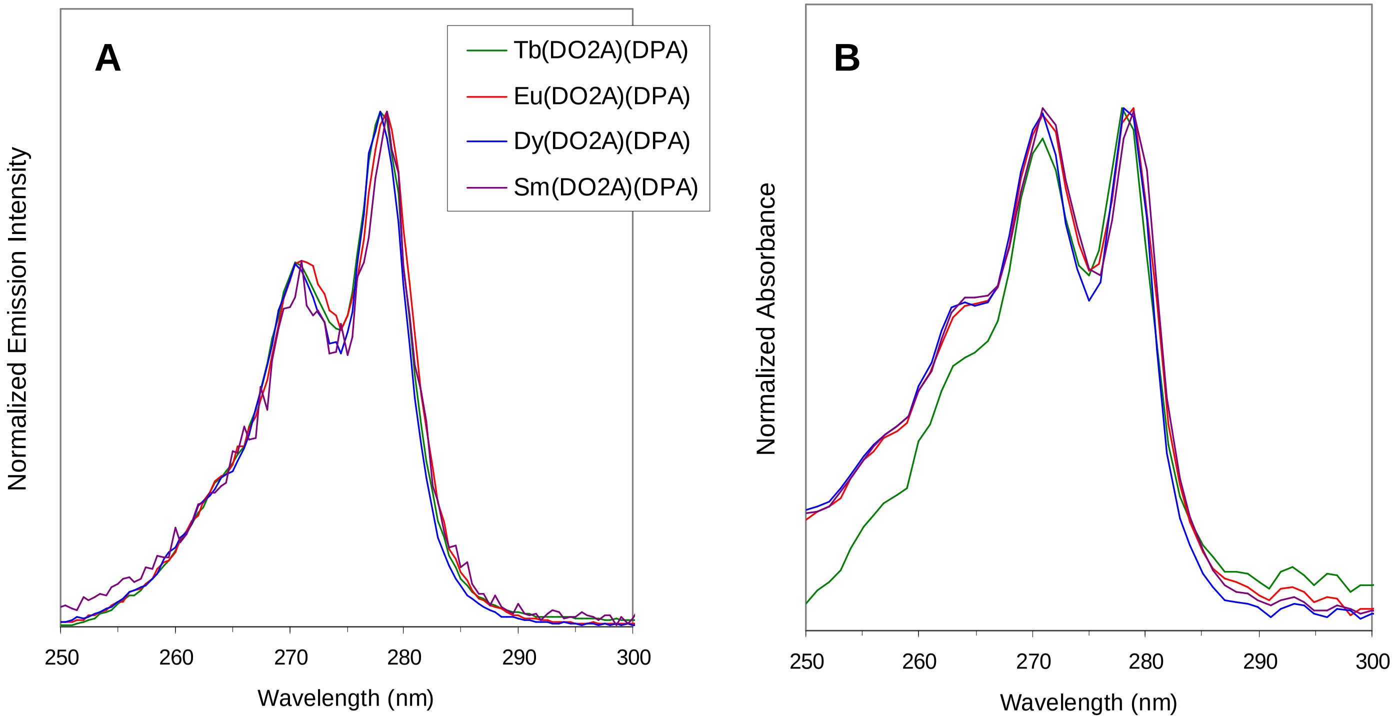

Figure 2.6. Normalized excitation (A) and absorption (B) spectra of Ln(DO2A)(DPA)$^-$ complexes, where Ln = Sm, Eu, Tb or Dy, at 10.0 μM in 0.1 M Tris, pH 7.9. Excitation wavelengths: λ_{Sm} = 600 nm, λ_{Eu} = 615 nm, λ_{Tb} = 544 nm, λ_{Dy} = 574 nm.

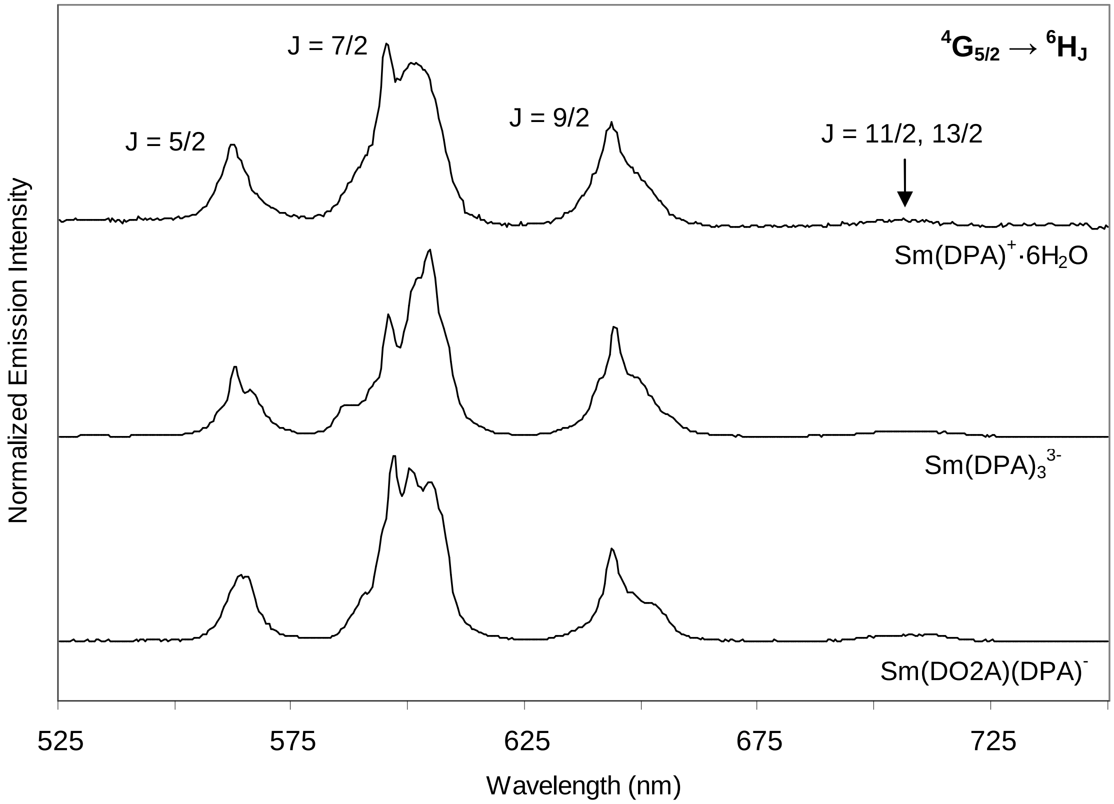

Figure 2.7. Emission spectra of samarium complexes, 10.0 μM in 0.2 M sodium acetate, pH 7.4 (λ_{ex} = 278 nm), showing characteristic splitting as a result of changes in the symmetry of the Sm^{3+} coordination sphere.

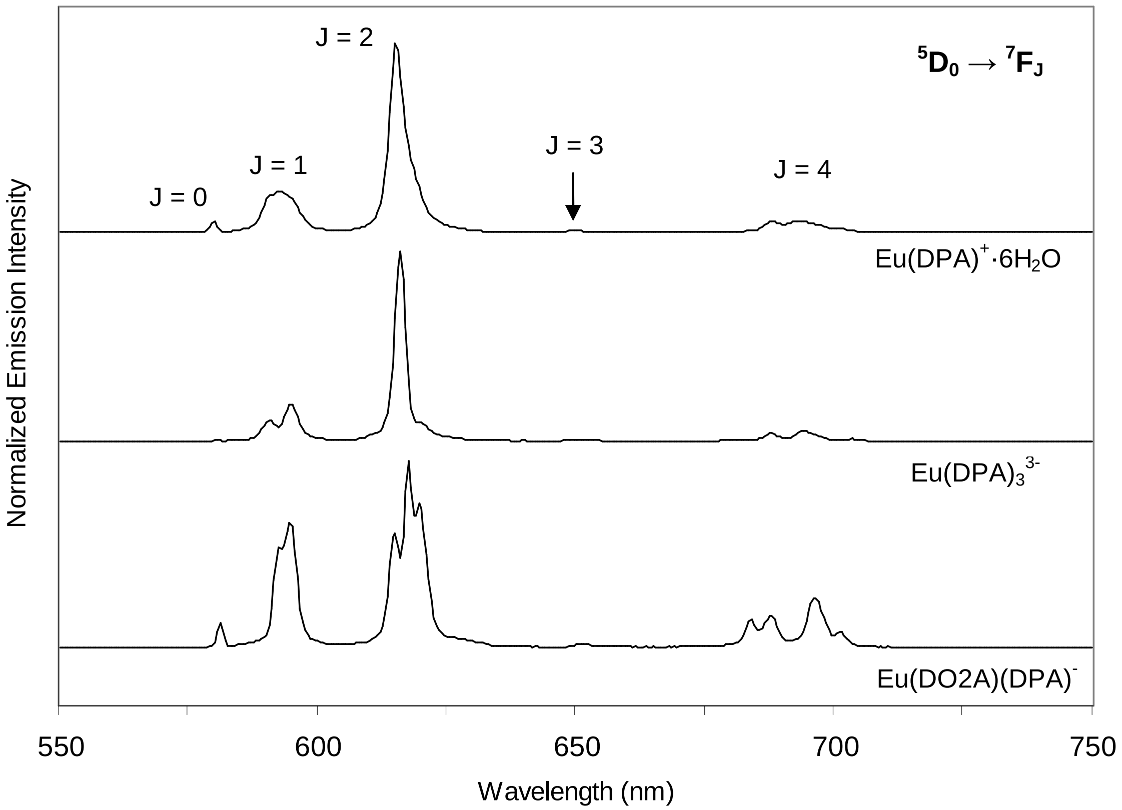

Figure 2.8. Emission spectra of europium complexes, 10.0 μM in 0.2 M sodium acetate, pH 7.4 (λ_{ex} = 278 nm).

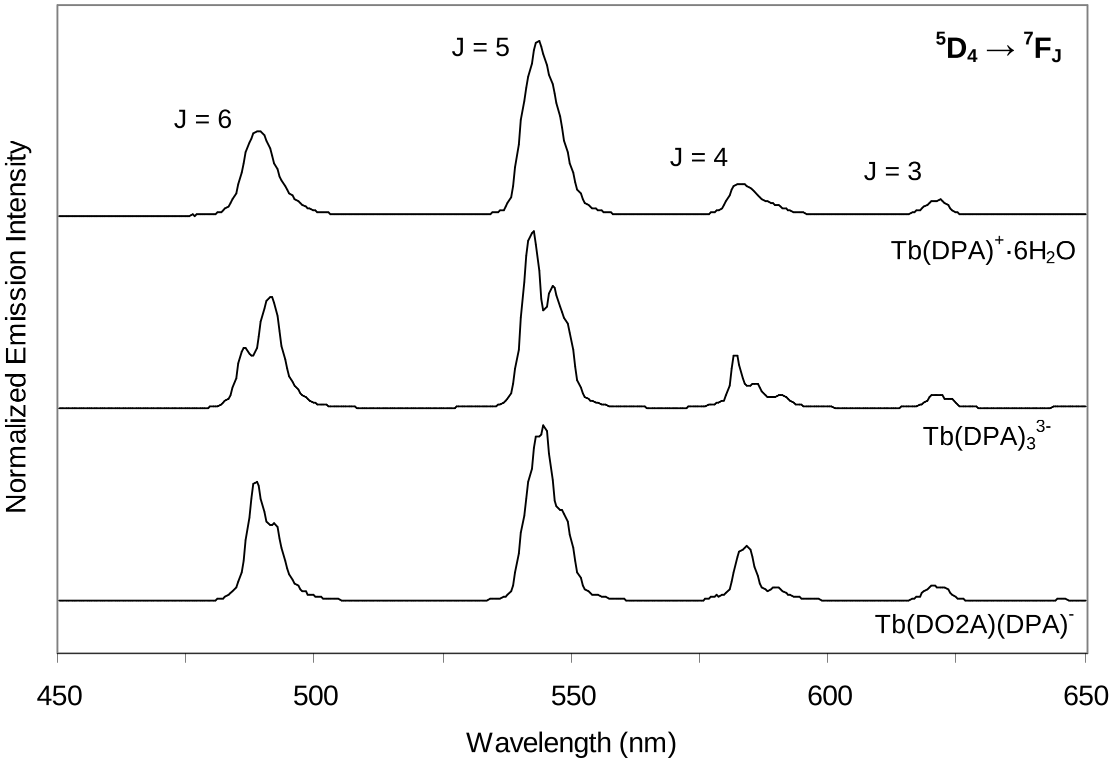

Figure 2.9. Emission spectra of terbium complexes, 10.0 μM in 0.2 M sodium acetate, pH 7.4 (λ_{ex} = 278 nm).

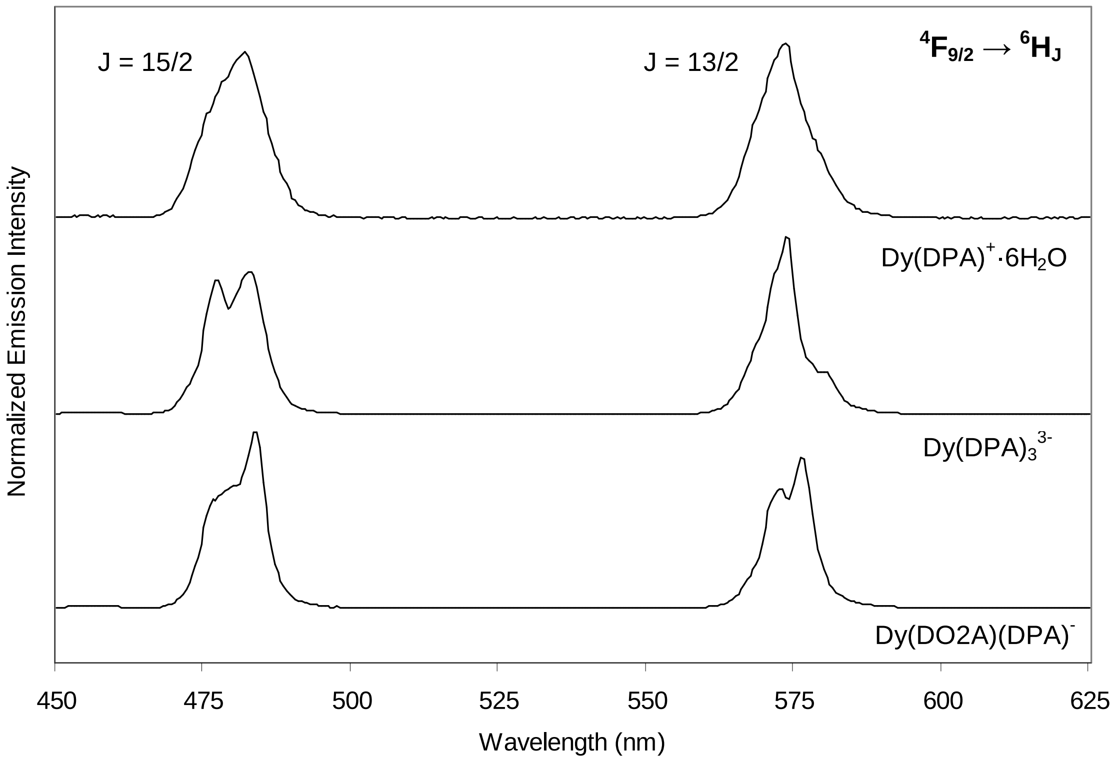

Figure 2.10. Emission spectra of dysprosium complexes, 10.0 μM in 0.2 M sodium acetate, pH 7.4 (λ_{ex} = 278 nm).

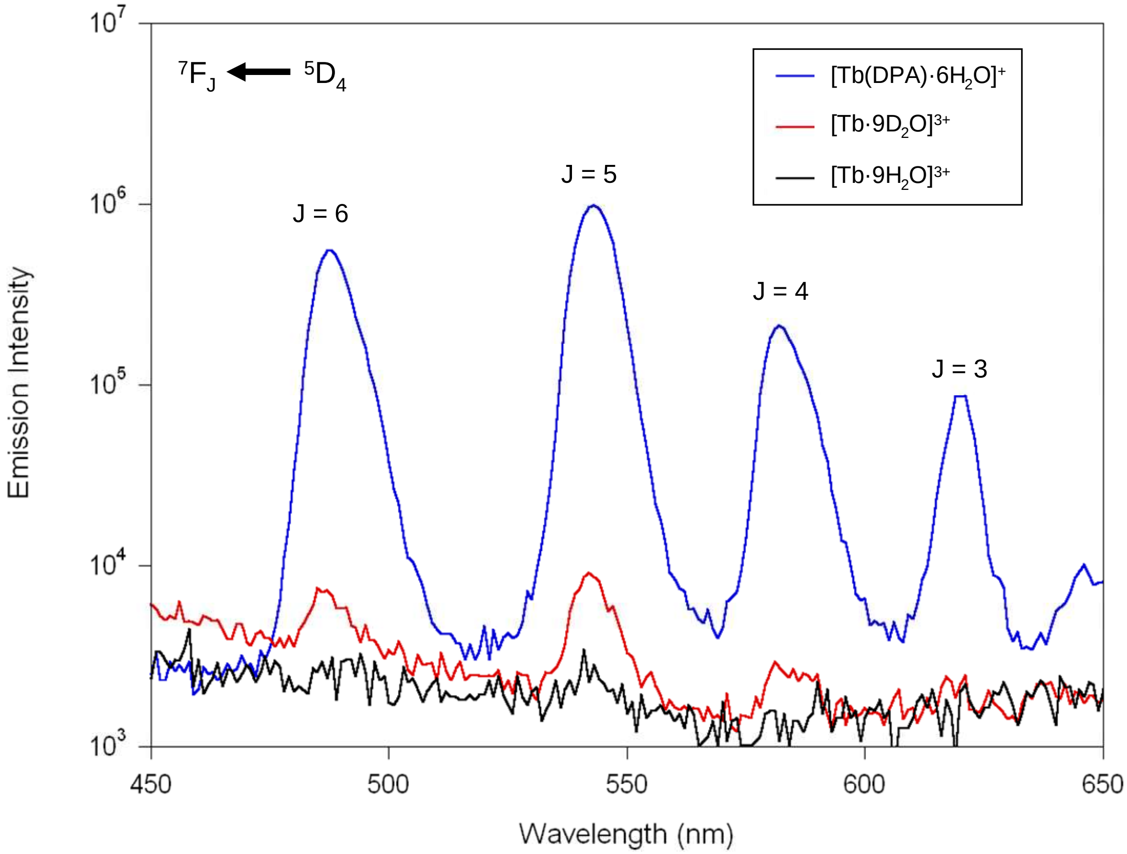

Figure 2.11. Effect of lanthanide sensitization compared to displacement of quenching solvent molecules. The emission spectrum of Tb^{3+} in D_2O shows a modest 3-fold increase in intensity (note Emission Intensity is a logarithmic scale), whereas the addition of one chromophore increases the terbium intensity by nearly three orders of magnitude.

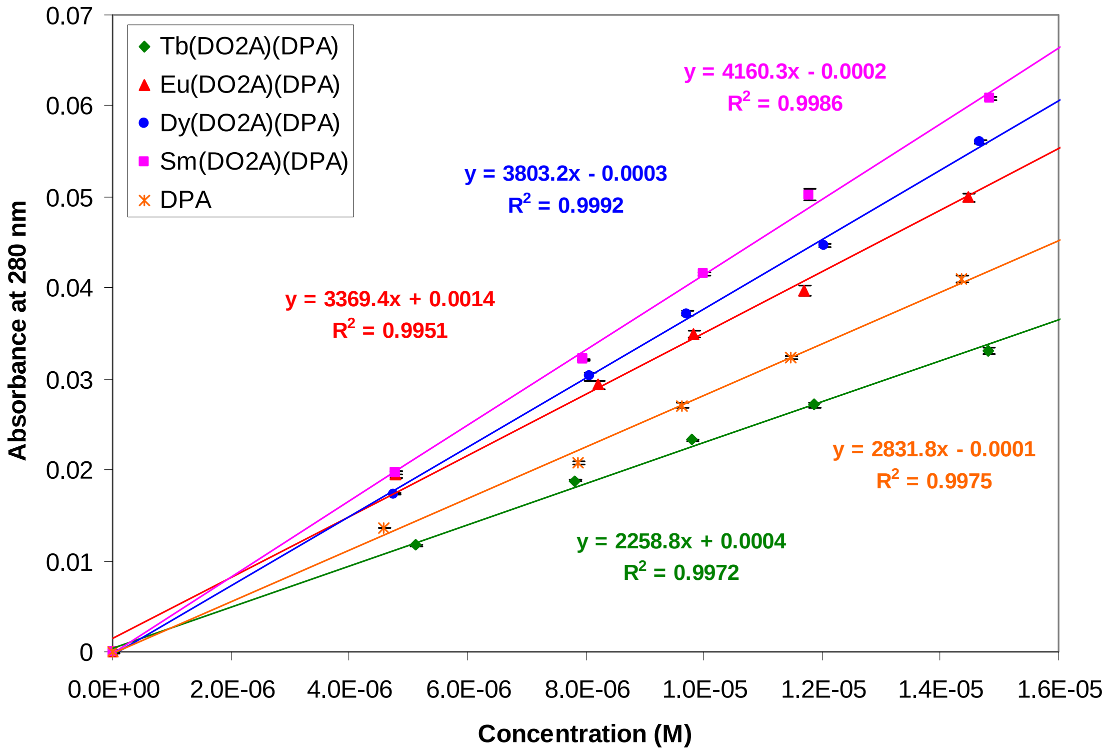

Figure 2.12. Linear fit of absorbance (λ_{abs} = 280 nm) versus concentration for the Ln(DO2A)(DPA)$^-$ complexes (Ln = Sm, Eu, Tb and Dy) in 0.1 M Tris buffer, pH 7.9.

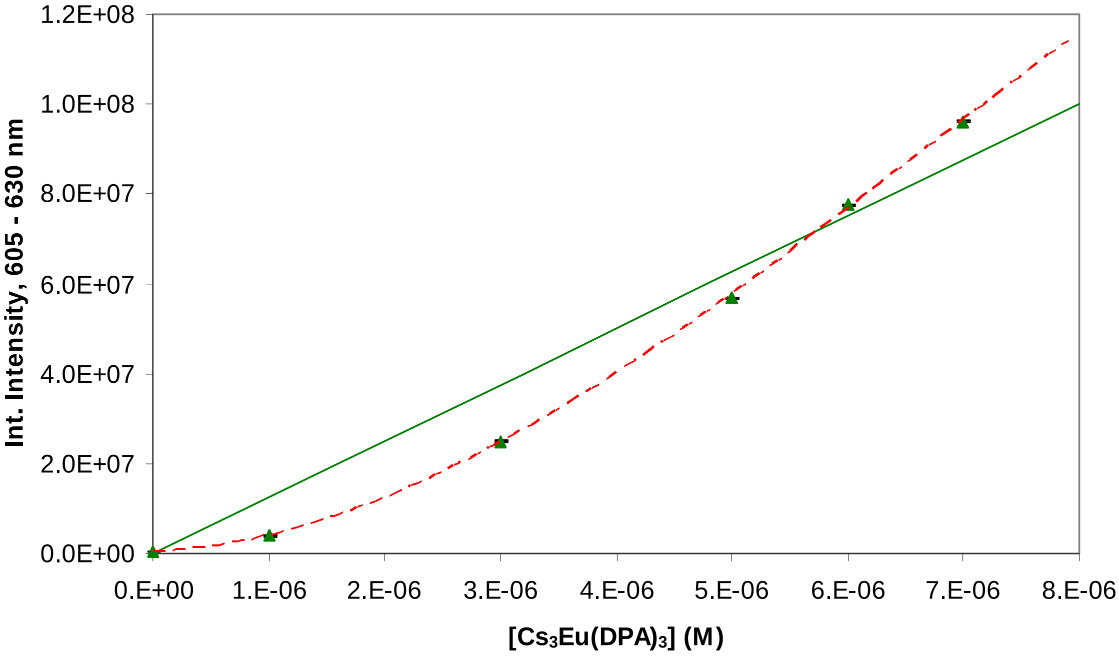

Figure 2.13. Fluorescence of $Cs_3Eu(DPA)_3$ in 0.1M Tris, pH 7.9, showing nonlinear behavior due to dissociation at low concentration.

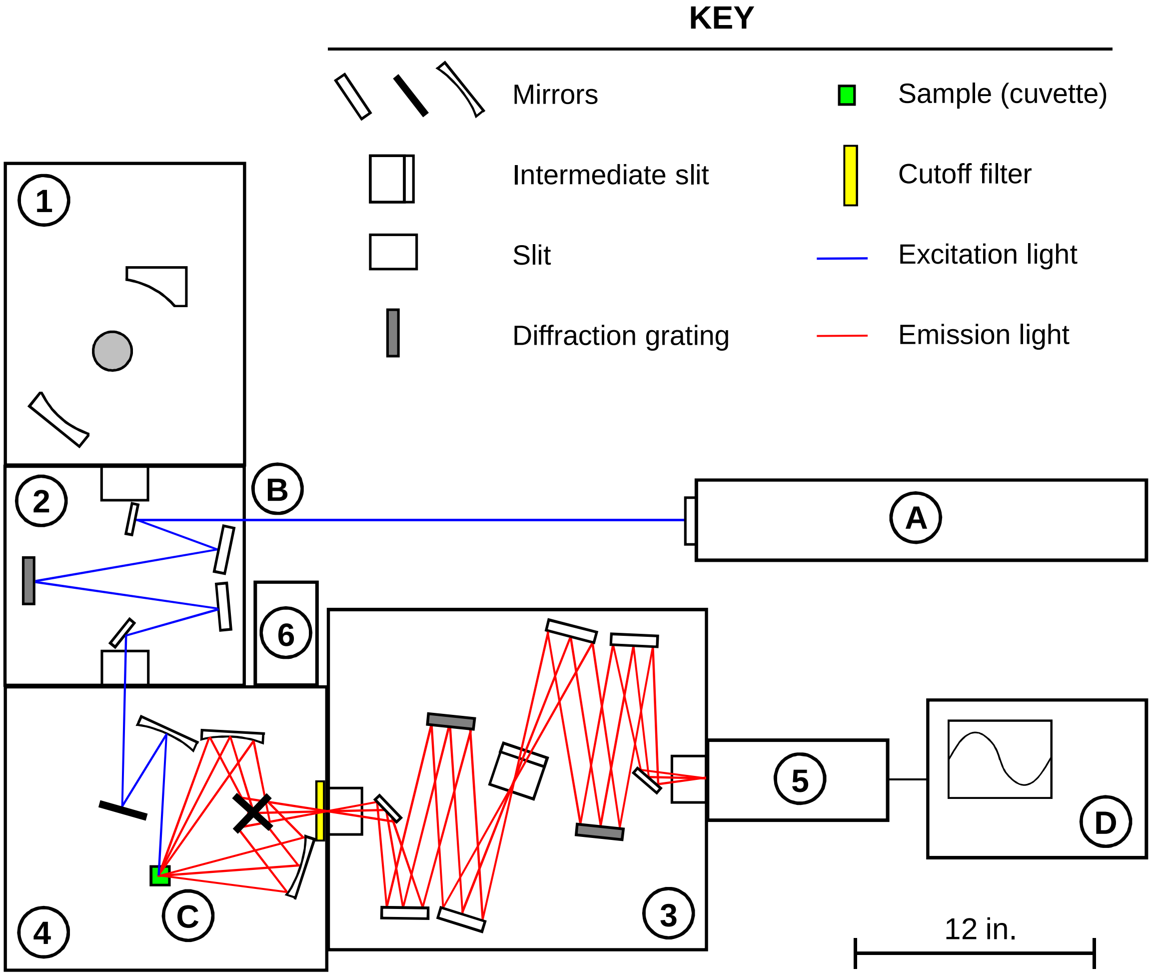

Figure 2.14. Schematic of the Fluorolog-3ᴛ Model FL3-12 spectrofluorometer used for lifetime measurements. Instead of the xenon lamp (1), a Nd:YAG laser with fourth-harmonic generation (266 nm) is used as the excitation source (A), so the excitation single monochromator (2) is no longer necessary as a wavelength selector and serves only as an alignment tool for the laser. The laser beam enters the excitation monochromator via a port on the side of the module (B), and is aligned to strike the center of the cuvette (C). An oscilloscope (D) is attached to the R928P photomultiplier tube (5) to obtain measurements of intensity as a function of time.

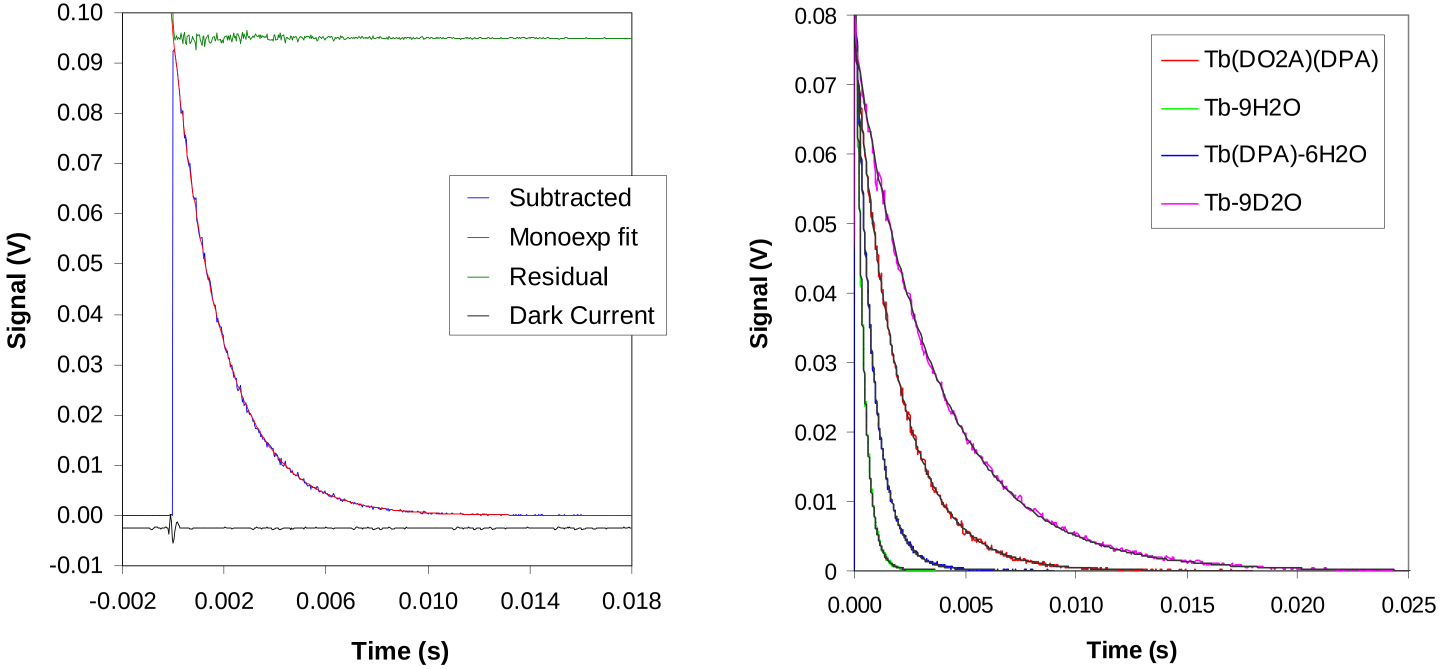

Figure 2.15. Exponential decay curves for lifetime measurements of various terbium complexes. Left: Example of raw data for 10 μM Tb(DO2A)(DPA), showing the adjusted decay curve (blue) following subtraction of the dark current (black) and the residual (green) resulting from subtraction. Right: Examples of final data and fits for several Tb complexes. Excitation at 266 nm (10 ns pulsed Nd:YAG laser), emission detected at 544 nm, sample concentrations 1 to 10 μM, pH 7.5 (adj with NaOH). These curves were fit to a monoexponential and used to determine the number of coordinated waters in the Tb^{3+} coordination sphere.

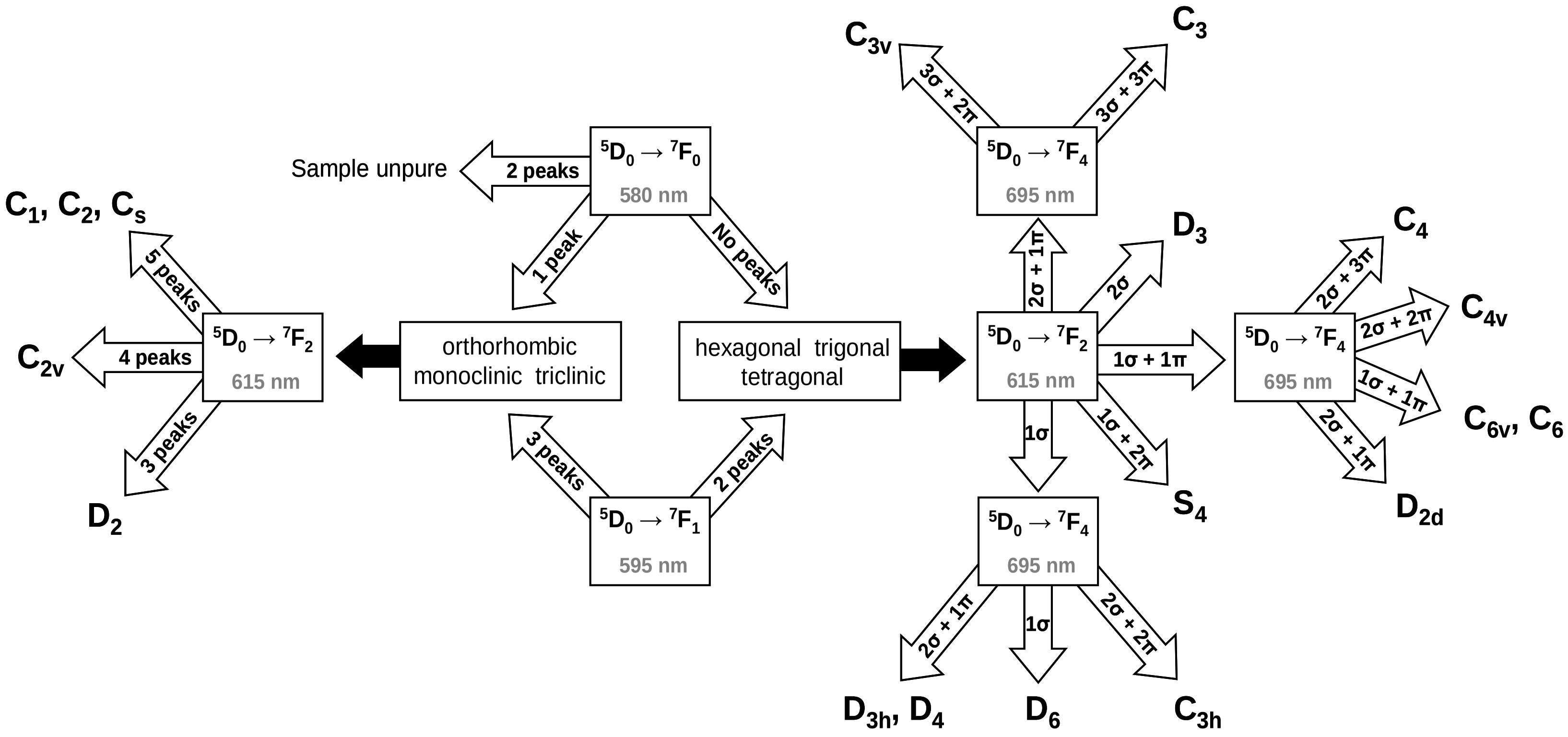

Figure 2.16. Scheme for point group determination based on selected transitions in the Eu^{3+} ion. Modified for luminescence spectra from reference 25.

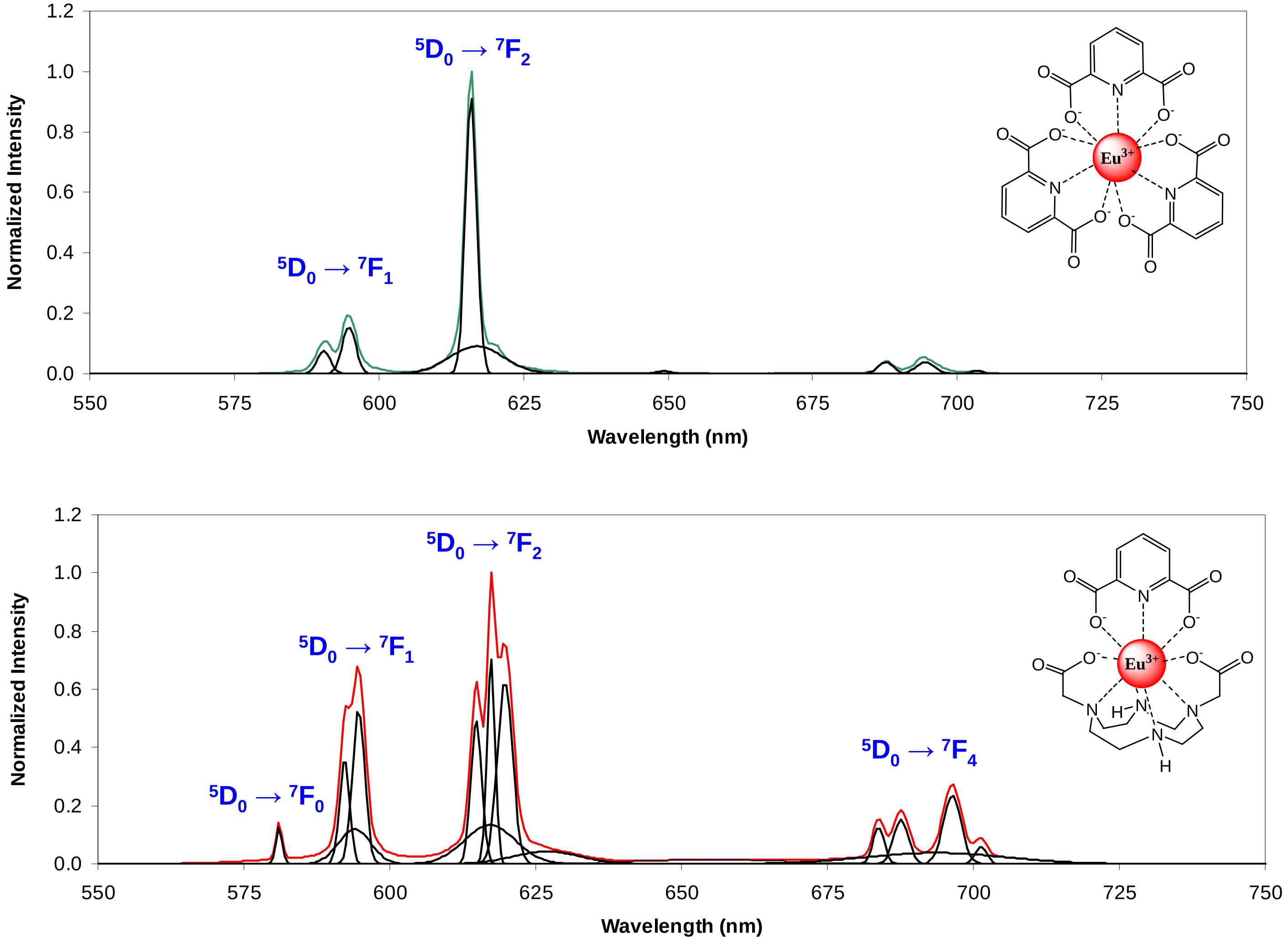

Figure 2.17. Emission spectra of Eu(DPA)$_3$ and Eu(DO2A)(DPA) complexes in green and red, respectively, with each transition deconvoluted into individual Stark sublevels via a sum of Gaussians program.

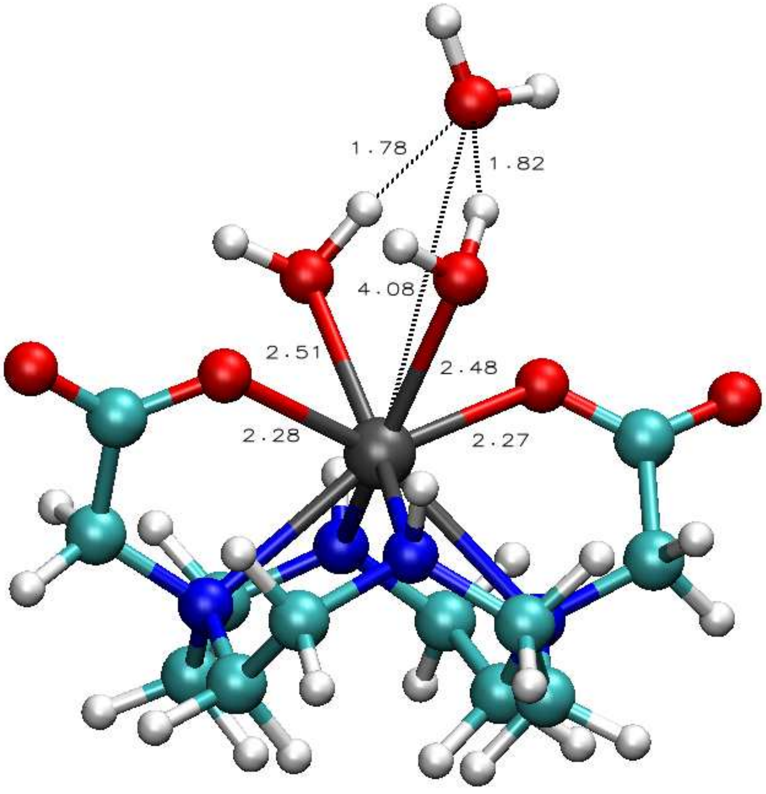

Figure 2.18. Theoretical model of Tb(DO2A)$^+$ complex, showing two solvent molecules in the terbium coordination sphere and one less strongly associated. Courtesy of J. Keith, Universität Ulm.

TABLES

Table 2.1. Crystallographic data for the five TBA•Ln(DO2A)(DPA) structures.

Ln	**Sm**	**Eu**	**Gd**	**Tb**	**Dy**
Formula	$[C_{19}H_{25}N_5O_8Sm]^-$ $[C_{16}H_{36}N]^+$• $0.27(C_2H_6O•O)$ $0.73(C_3H_6O)$ $2(H_2O)$	$[C_{19}H_{25}N_5O_8Eu]^-$ $[C_{16}H_{36}N]^+$• $0.68(C_3H_8O)$ $0.32(C_3H_6O)$ $3(H_2O)$	$[C_{19}H_{25}N_5O_8Gd]^-$ $[C_{16}H_{36}N]^+$• $0.38(C_3H_6O•O)$ $0.62(C_3H_6O)$ $2(H_2O)$	$[C_{19}H_{25}N_5O_8Tb]^-$ $[C_{16}H_{36}N]^+$• $0.47(C_3H_8O)$ $0.53(C_3H_6O)$ $3(H_2O)$	$[C_{19}H_{25}N_5O_8Dy]^-$ $[C_{16}H_{36}N]^+$• $2(C_3H_8O)$ $3(H_2O)$
M_w	939.36	957.23	946.79	964.94	966.51
Crystal system	Monoclinic	Triclinic	Monoclinic	Monoclinic	Monoclinic
Space group	$P2_1/c$	P1	$P2_1/c$	$P2_1/c$	$P2_1/c$
a (Å)	13.0658(4)	13.1473(4)	13.1910(5)	13.1047(5)	13.1742(4)
b (Å)	13.4504(4)	13.2269(4)	13.4544(5)	13.3397(5)	13.1860(4)
c (Å)	26.1778(7)	26.2248(8)	26.1712(9)	26.0901(9)	26.1130(8)
β (°)	90.3240(10)	90.0540(10)	90.368(2)	90.0130(10)	90.3720(10)
V ($Å^3$), Z	4600.4(2)	4560.4(2)	4644.7(3)	4560.9(3)	4536.1(2)
λ (Å)	0.71073	0.71073	0.71073	0.71073	0.71073
D_c (Mg/m^3)	1.356	1.394	1.354	1.405	1.415
μ,Mo-Kα (mm^{-1})	1.336	1.438	1.487	1.613	1.710
T (K)	100(2)	100(2)	100(2)	100(2)	100(2)
R_1, wR_2‡	0.0422, 0.0734	0.0437, 0.0750	0.0302, 0.0482	0.0384, 0.0639	0.0408, 0.0721

‡ Structure refined on F^2 using all reflections: $wR_2 = [\Sigma[w(F^2 - F_c^2)^2]/\Sigma w(F^2)^2]^{1/2}$, where $w^{-1} = [\Sigma(F^2) + (aP)^2 + bP]$ and $P = [\max(F^2,0) + 2F_c^2]/3$.

Table 2.2. Relevant bond distances for various gadolinium complexes.

	Gd(DO2A)(DPA)	**[Gd(DO3A)]$_3$•Na$_2$CO$_3$**[†]	**Na[Gd(H$_2$O)(DOTA)]** [†]
Gd--N1	2.6607(9)	2.63	2.656(3)
Gd--N2	2.5960(9)	2.60	2.688(3)
Gd--N3	2.6727(9)	2.59	2.645(3)
Gd--N4	2.5816(9)	2.56	2.661(4)
Gd--O1	2.3941(7)	2.35	2.379(3)
Gd--O3	2.3850(7)	2.34	2.362(3)
Gd--O7		2.35	2.359(3)
Gd--O9			2.370(3)

[†] Reference 14

Note: Numbering of O atoms was modified in the DO2A complex to be consistent with the reported DO3A and DOTA complexes.

Table 2.3. Crystallographic data for the three TBA•Eu(DO2A)(DPA) structures.

Temp	**100 K**	**200 K**	**300 K**
Formula	$[C_{19}H_{25}N_5O_8Eu]^-$ $[C_{16}H_{36}N]^+$• C_3H_6O • 3.68(H_2O)	$[C_{19}H_{25}N_5O_8Eu]^-$ $[C_{16}H_{36}N]^+$• C_3H_6O • 3.68(H_2O)	$[C_{19}H_{25}N_5O_8Eu]^-$ $[C_{16}H_{36}N]^+$• C_3H_6O • 3.68(H_2O)
M_w	970.23	970.23	949.07
Crystal system	Monoclinic	Monoclinic	Monoclinic
Space group	$P2_1/c$	$P2_1/c$	$P2_1/c$
a (Å)	13.0309(5)	13.1516(5)	13.3306(9)
b (Å)	13.4740(5)	13.5276(5)	13.4557(9)
c (Å)	26.1088(9)	26.1946(9)	26.3443(17)
β (°)	90.600(2)	90.701(2)	90.450(3)
V (Å^3), Z	4583.9(3)	4659.9(3)	4725.3(5)
λ (Å)	0.71073	0.71073	0.71073
D_c (Mg/m^3)	1.406	1.383	1.334
μ,Mo-Kα (mm^{-1})	1.432	1.409	1.386
T (K)	100(2)	200(2)	300(2)
R_1, wR_2[‡]	0.0341, 0.0624	0.0337, 0.0550	0.0469, 0.0623

[‡] Structure refined on F^2 using all reflections: $wR_2 = [\Sigma[w(F^2 - F_c^2)^2]/\Sigma w(F^2)^2]^{1/2}$, where $w^{-1} = [\Sigma(F^2) + (aP)^2 + bP]$ and $P = [\max(F^2,0) + 2F_c^2]/3$.

Table 2.4. Molar extinction coefficients of the Ln(DO2A)(DPA)$^-$ complexes (Ln = Sm, Eu, Tb, Dy) and the DPA^{2-} anion.

Complex	Buffer	λ_{abs} (nm)	Temp (℃)	pH	$\boldsymbol{\varepsilon}_{Exp}$ (M^{-1}cm$^{-1)}$
Sm(DO2A)(DPA)$^-$	0.1 M Tris	280	22.0	7.49	4160 ± 10
Eu(DO2A)(DPA)$^-$			22.1	7.46	3369 ± 24
Tb(DO2A)(DPA)$^-$			22.0	7.43	2259 ± 10
Dy(DO2A)(DPA)$^-$			22.1	7.49	3803 ± 2
DPA^{2-}			22.3	7.50	2832 ± 21

Table 2.5. Luminescence quantum yield data, 0.1 M Tris buffer, L-Trp standard.

Complex	Temp (℃)	pH	Φ_L (x 10^{-3})
$Sm(DO2A)(DPA)^-$	25.4 ± 0.3	7.93 ± 0.02	1.09 ± 0.03
$Eu(DO2A)(DPA)^-$	24.7 ± 0.1	7.92 ± 0.02	7.51 ± 0.03
$Tb(DO2A)(DPA)^-$	24.8 ± 0.2	7.93 ± 0.01	110 ± 2
$Dy(DO2A)(DPA)^-$	25.6 ± 0.3	7.87 ± 0.02	5.58 ± 0.07

Table 2.6. Ligand energy levels and lanthanide ion resonance levels in the absorbance-energy transfer-emission (AETE) mechanism of DPA-sensitized lanthanide luminescence.

Ligand Energy Level (cm^{-1})		Ln^{3+} Ion Resonance Level (cm^{-1})	
DPA Triplet	26,600 [32]	Sm^{3+} $^4G_{5/2}$	17,900 [35]
		Eu^{3+} $^5D_0$	17,264 [36]
		Tb^{3+} $^5D_4$	20,500 [34]
		Dy^{3+} $^4F_{9/2}$	21,100 [35]

Table 2.7. Luminescent lifetime measurements[a] of various terbium complexes.

complex[b]	τ_{H_2O} (ms)	τ_{D_2O} (ms)	q[c]
$[Tb(H_2O)_9]^{3+}$	0.4	3.4	8.8 ± 1.1
$[Tb(DPA)(H_2O)_6]^+$	0.6[d]	3.5	5.6 ± 0.7
$[Tb(DO2A)(H_2O)_3]^+$	1.1	2.6	2.4 ± 0.3
$[Tb(DO2A)(DPA)]^-$	1.9	2.2	0.3 ± 0.0

[a] Excitation at 266 nm (10 ns, pulsed Nd:YAG laser), emission detection at 544 nm, sample concentrations 1 to 10 μM, pH 7.5 (adjusted with NaOH).

[b] Waters included assuming that the Tb^{3+} ion is 9-coordinate.

[c] The number of water molecules, q, in the Tb^{3+} coordination sphere, where

$$q = A_{Ln}\,(\tau^{-1}_{H_2O} - \tau^{-1}_{D_2O})$$

and A_{Tb} = 4.6 or 4.2 ± 0.5 ms^{-1} per bound water molecule for complexes with and without DO2A, respectively.

[d] See reference 45.